THERMOELECTRIC EFFECTS IN MESOSCOPIC PHYSICS

A THESIS SUBMITTED TO
THE GRADUATE SCHOOL OF NATURAL AND APPLIED SCIENCES
OF
THE MIDDLE EAST TECHNICAL UNIVERSITY

BY

M. ALİ ÇİPİLOĞLU

IN PARTIAL FULFILLMENT OF THE REQUIREMENTS FOR THE DEGREE OF

DOCTOR OF PHILOSOPHY

IN

THE DEPARTMENT OF PHYSICS

JANUARY 2004

Approval of the Graduate School of Natural and Applied Sciences.

Prof. Dr. Canan Özgen
Director

I certify that this thesis satisfies all the requirements as a thesis for the degree of Doctor of Philosophy.

Prof. Dr. Sinan Bilikmen
Head of Department

This is to certify that we have read this thesis and that in our opinion it is fully adequate, in scope and quality, as a thesis for the degree of Doctor of Philosophy.

Dr. Sadi Turgut
Supervisor

Examining Committee Members

Prof. Dr. Mehmet Tomak

Prof. Dr. Bülent Akınoğlu

Assoc. Prof. Dr. Hatice Kökten

Assist. Prof. Dr. Ceyhun Bulutay

Dr. Sadi Turgut

ABSTRACT

THERMOELECTRIC EFFECTS IN MESOSCOPIC PHYSICS

Çipiloğlu, M. Ali

Ph.D., Department of Physics

Supervisor: Dr. Sadi Turgut

January 2004, 69 pages

The electrical and thermal conductance and the Seebeck coefficient are calculated for one-dimensional systems, and their behavior as a function of temperature and chemical potential is investigated. It is shown that the conductances are proportional to an average of the transmission probability around the Fermi level with the average taken for the thermal conductance being over a wider range. This has the effect of creating less well-defined plateaus for thermal-conductance quantization experiments.

For weak non-linearities, the charge and entropy currents across a quantum point contact are expanded as a series in powers of the applied bias voltage and the temperature difference. After that, the expansions of the Seebeck voltage

in temperature difference and the Peltier heat in current are obtained.

Also, it is shown that the linear thermal conductance of a quantum point contact displays a half-plateau structure, almost flat regions appearing around half-integer multiples of the conductance quantum. This structure is investigated for the saddle-potential model.

Keywords: quantized conductance, thermopower, thermoelectric effect, Peltier effect, Seebeck effect, quantum point contacts, two-dimensional electron gas

ÖZ

MEZOSKOPİK FİZİKTE TERMOELEKTRİK ETKİLER

Çipiloğlu, M. Ali

Doktora, Fizik Bölümü

Tez Yöneticisi: Dr. Sadi Turgut

Ocak 2004, 69 sayfa

Tek boyutlu için elektrik, ısı iletkenlikleri ve Seebeck katsayısı hesaplandı. Hesaplanan bu değerlerin sıcaklık ve kimyasal potansiyele göre değişimleri incelendi. Elektrik ve ısı iletkenliklerinin, Fermi seviyesi civarındaki geçiş olasılığı ortalamasıyla doğru orantılı olduğu ve ısı iletkenliği için çizilen grafiklerde oluşan platoların elektrik iletkenlik için çizilenlere göre daha az belirgin olduğu gözlendi.

Doğrusal olmayan durumlar için kuantum nokta kontaktların yük ve entropi akımları uygulanan potansiyel farkı ve sıcaklık cinsinden seri açılımı yapıldı. Sıcaklık farkı cinsinden Seebeck gerilimi ve akım cinsinden de Peltier

ısısı elde edildi.

Son olarak, kuantum nokta kontakt için doğrusal ısı iletkenliğinin yarım plato yapısı gösterdiği ve bu yapının yaklaşık olarak iletkenlik kuantumunun yarısı civarında ortaya çıktığı gözlendi.

Anahtar Kelimeler: kuantumlaşmış iletkenlik, Seebeck etkisi, Peltier etkisi, kuantum nokta kontakt, iki boyutlu elektron gazı, termoelektrik etkiler

ACKNOWLEDGMENTS

I would like to thank Prof. Dr. Mehmet Tomak and Dr. Sadi Turgut for the discussion and their support.

TABLE OF CONTENTS

ABSTRACT iii

ÖZ v

ACKNOWLEDGMENTS vii

TABLE OF CONTENTS viii

LIST OF FIGURES x

LIST OF SYMBOLS xiii

CHAPTER

I INTRODUCTION 1

I.1 Ballistic Transport and Landauer-Büttiker Formalism . 3

I.1.1 Single-Channel Case 4

I.1.2 The Multi-Channel Case 7

I.2 Thermoelectricity 12

II ELECTRICAL AND THERMAL TRANSPORT COEFFICIENTS IN ONE DIMENSION 16

II.1 Introduction 16

II.2 Transport Coefficients 17

II.3 Low Temperature Case 19

II.4 Intermediate Temperatures 20

II.5 Variation with Chemical Potential 25

II.6 Conclusion 28

III NONLINEAR SEEBECK AND PELTIER EFFECTS IN QUANTUM POINT CONTACTS 29

III.1 Introduction 29

III.2 Model 31
III.3 Seebeck Effect 35
III.4 Peltier Effect 42
III.4.1 High-order nonlinearity in Peltier effect at small temperatures 44
III.5 Conclusions 47
IV HALF STEPS IN THE LINEAR THERMAL CONDUCTANCE OF QUANTUM POINT CONTACTS 49
IV.1 Introduction 49
IV.2 Theory 51
IV.3 Results and Discussion 53
IV.4 Conclusions 63
REFERENCES 65
VITA 69

LIST OF FIGURES

I.1 Schematic view of the metal gate used to define a constriction to observe conductance quantization 3

I.2 A conductor with one scatterer having a transmission probability of T is connected between two large contacts through two leads, and this system can be reduced to the barrier problem. . 5

I.3 *a.* Closed circuit. Basic thermoelectric circuits. If 1 and 2 are different conducting materials, a thermoelectric current will flow. *b.* Open circuit. The thermoelectric potential difference generated, ΔV_{12}, will be proportional to ΔT if $\frac{\Delta T}{T} \ll 1$. 13

I.4 Peltier heat. If an electric current I passed through the junction, heat will be evolved or absorbed, depending on the direction of I. The Peltier heat, Π_{12}, will be positive if heat is evolved at the junction in the figure, or vice versa. 14

II.1 Transmission probability for $\ell = 18\frac{\hbar}{\sqrt{2mV_0}}$. 21

II.2 Conductances as a function of temperature for two different values of chemical potential. Dotted curves are for the electrical conductance [$G_{\rm el}/(2e^2/h)$ is plotted], and the solid ones are for the thermal conductance [$G_{\rm th}/(2\pi^2 k_B^2 T/3h)$ is plotted.] The lower two curves are for $\mu = 1.2V_0$ and the upper curves are for $\mu = 1.3V_0$. Those values of μ are shown in Figure II.1 as circles. 22

II.3 Lorenz ratio divided by its ideal value for $\mu = 1.2V_0$ (upper curve) and for $\mu = 1.3V_0$ (lower curve). 23

II.4 The Seebeck coefficient [Se/k_B is plotted] for $\mu = 1.2V_0$ (lower curve) and for $\mu = 1.3V_0$ (upper curve). 24

II.5 The Electrical conductance (dotted curve) [$G_{\rm el}/(2e^2/h)$ is plotted] and the thermal conductance [$G_{\rm th}/(2\pi^2 k_B^2 T/3h)$ is plotted] as a function of the chemical potential μ at the temperature $k_B T = 0.01V_0$. 26

II.6 Lorenz ratio divided by its ideal value (up) and the Seebeck coefficient (down) as a function of the chemical potential μ at the temperature $k_B T = 0.01V_0$. 27

III.1 The third order Seebeck coefficient, $\sigma_3 = (-e)\theta_A^2/k_B\ S_3$, is plotted as a function of average chemical potential $\overline{\mu}$ for $\omega_y/\omega_x = 6$ and $k_B\overline{\theta}/\hbar\omega_y$ = 0.01, 0.02, 0.04, 0.08, 0.105 and 0.125 (from bottom to top). Each curve is shifted by 0.05 units for clarity. . 37
III.2 For comparison the linear Seebeck coefficient, $\sigma_1 = (-e)/k_B\ S_1$, is plotted for the same set of parameters. Each curve is shifted by 0.02 units and the temperature increases from bottom to top. 38
III.3 The third order Seebeck coefficient, $\sigma_3 = (-e)\theta_A^2/k_B\ S_3$, is plotted as a function of average chemical potential $\overline{\mu}$ for $k_B\overline{\theta}/\hbar\omega_y = 0.04$ and $\omega_y/\omega_x = 1.5$, 3, 6 and 12 (from top to bottom) respectively. Each plot is shifted by 0.025 units for clarity. 40
III.4 For comparison, the linear Seebeck coefficient, $\sigma_1 = (-e)/k_B\ S_1$, is plotted for the same set of parameters. Each plot is shifted by 0.2 units and ω_y/ω_x ratio increases from top to bottom. . . . 41
III.5 The third-order Peltier coefficient Π_3 (in arbitrary units) is plotted as a function of average chemical potential $\overline{\mu}$ for $\omega_y/\omega_x = 6$ and different values of temperatures ($k_B\overline{\theta}/\hbar\omega_y$ values are indicated in the figure). 45
III.6 The third order Peltier coefficient Π_3 is plotted as a function of average chemical potential $\overline{\mu}$ for $k_B\overline{\theta}/\hbar\omega_y = 0.04$ and different values of ω_y/ω_x whose values are indicated in the figure. 46

IV.1 (a) The electrical conductance (dotted) in units of $2e^2/h$ and the thermal conductance (solid) in units of K_0 plotted as a function of the chemical potential. The curves are for (from bottom to top) ω_y/ω_x = 1, 3, 10, 30, 100 and 300 and $k_B\theta/\hbar\omega_y = 0.05$. Different curves are shifted vertically for the sake of clarity. (b) The derivative of the thermal conductance (in units of $K_0/\hbar\omega_y$) for the same parameter values. The ratio ω_y/ω_x increases from the bottom to the top and different curves are shifted vertically by 2 units. 53
IV.2 (a) The electrical conductance (dotted) in units of $2e^2/h$ and thermal conductance (solid) in units of K_0 plotted as a function of the chemical potential. The curves are obtained for (from bottom to top) $k_B\theta/\hbar\omega_y$ =0.01, 0.03, 0.06, 0.1, 0.15 and 0.2 and $\omega_y/\omega_x = 3$. Different curves are shifted vertically for the sake of clarity. (b) The derivative of the thermal conductance with respect to chemical potential (in units of $K_0/\hbar\omega_y$) for the same parameter values. Different curves are shifted vertically by 2 units for clarity and the temperature increases from the bottom to the top. 54
IV.3 (a) The thermal conductance, K, and (b) its derivative, $\partial K/\partial\mu$, around the second step (step between $n = 1$ and $n = 2$ plateaus) for different values of $k_B\theta/\hbar\omega_x$ ratio. Values of that ratio are indicated in the graphs. 55

IV.4 Currents between a hot (above) and a cold conductor (middle). The transmission sum function, $T(E)$, and the energy-resolved heat current (shaded curve) are plotted below. The current node, E_{CN}, the energy at which the current is zero, is present due to the restriction that the total particle current is zero. The relative shift of the Fermi levels due to the Seebeck effect is not shown. 60
IV.5 The energy of the current node as a function of the chemical potential for the first step. The effects of the other steps are ignored (i.e., $\omega_y \gg \omega_x$). The curves are obtained for (from bottom to top) $k_B\theta/\hbar\omega_x$ =0.02, 0.08, 0.2, 0.4, 0.6 and 0.8. For the lowest curve, E_{CN} is roughly equal to μ. 64

LIST OF SYMBOLS

1D	One Dimensional
2D	Two Dimensional
2DEG	Two Dimensional Electron Gas
emf	Electro Motive Force
LHS	Left-hand side
RHS	Riht-hand side

CHAPTER I

INTRODUCTION

Conductance properties of extremely narrow constrictions is a rapidly developing field of research. Recent advances in fabrication and material growth technologies have made possible the production of devices whose dimensions are intermediate between the macroscopic and the microscopic length scales. Such devices are called as mesoscopic. What makes important these mesoscopic devices is that at these scales, some extraordinary behaviors appear; a mixture of classical and quantum mechanical rules are valid, i.e, an electron no longer behaves simply as a particle, but begins to exhibit quantum-mechanical effects.

Although some of pioneering experiments in this field were performed using metallic conductors, most of the recent work on mesoscopic conductors has largely been based on GaAs-AlGaAs heterojunctions where a thin two-dimensional conducting layer is formed at the interface between GaAs and

AlGaAs. These semiconductor materials are very special for forming two-dimensional electron gas (2DEG) because of two important properties. First, 2DEG in a GaAs-AlGaAs heterojunction has Fermi wavelength which is about a hundred times larger than in a metal. Second, in these heterolayers electrons have extremely low scattering rates and high mobility (at low temperatures).

These properties make it possible to study a constriction with an opening comparable to the Fermi wavelength (and much smaller than the mean free path). Such a constriction is called a quantum point, or ballistic, contact. If the width of the constriction can be varied, one can adjust the position of the one-dimensional electron-energy subbands (modes, channels) with respect to Fermi level. Such a quantum point contact of adjustable width can usually be achieved by using split-gate technique developed by Thornton T. J. *et al*[1]. A typical geometry is shown in Figure I.1. Two metal gates are deposited on top of the heterostructure. A narrow channel, called as the point contact, is defined by the application of a negative voltage to the gate which depletes the electrons of the 2DEG beneath it.

In 1988, van Wees *et al.*[2] and Wharam *et al.*[3] independently reported low-temperature conductance versus gate voltage data in split-gate structures that exhibited conductance steps quantized in integer multiples of conductance quantum $G_0 = 2e/h^2$. This phenomenon is usually treated with the Landauer-Büttiker formalism[4, 5] which explains it in a very simple way.

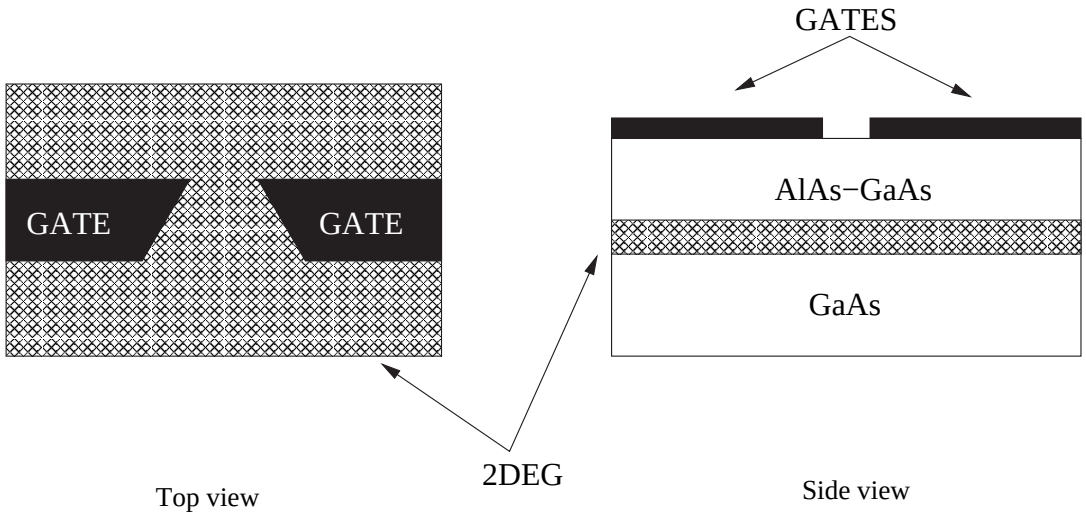

Figure I.1: Schematic view of the metal gate used to define a constriction to observe conductance quantization

I.1 Ballistic Transport and Landauer-Büttiker Formalism

If the mean free path L is larger than the both width and length of the channel, carriers can pass through the channel without suffering collisions of any kind. As mentioned in the previous section, the most dramatic consequence of this regime is the conductance quantization at integer multiples of $2e/h^2$[2, 3].

One of the formulas is the Landauer formula which can be used to explain why the conductance of a short narrow wire is quantized. Considering the relation between the conductance of a one-dimensional (1D) wire and the transmission and reflection probabilities at the Fermi level, Landauer[4] derived a formula which is based on scattering properties of the system. Later on Büttiker[5] generalized this idea again for the mesoscopic systems, and the resulting Landauer-Büttiker formalism is introduced in the following section.

Many theoretical studies[6, 7, 8, 9, 10] have been done within the Landauer-Büttiker formalism to investigate the transport through a quantum point contact between two electron-gas reservoirs, the formalism has also been used in interpretation and analysis of some experimental studies[2, 3, 11, 12, 13, 14, 15].

I.1.1 Single-Channel Case

Consider a general barrier problem for a 1D conductor shown in Fig. I.2. Let an ideal lead, in which electrons travel without scattering, is attached between two perfect reservoirs with electrochemical potentials μ_L and $\mu_R = \mu_L + eV$ respectively, where V is the applied voltage. Also let T and $R = 1 - T$ be the transmission and reflection probabilities, respectively, of a scatterer between the ideal leads. Then the total current flowing across the system is given by

$$I = (-e)\upsilon_F \frac{\partial n}{\partial E} T(\mu_L - \mu_R) \qquad , \tag{I.1}$$

where,

$$\frac{\partial n}{\partial E} = \frac{2}{h\upsilon_F}$$

is the density of states for electrons moving from left to right, the factor 2 comes from spin degeneracy, and υ_F is the Fermi velocity. Since, the conductance is the ratio of the current to the voltage applied across the system and remembering the voltage difference between L and R is

$$V_{RL} = \frac{\mu_L - \mu_R}{(-e)} \qquad ,$$

the two terminal conductance can be written as

$$G = \frac{I}{V_{RL}} = \frac{2e^2}{h} T \qquad . \tag{I.2}$$

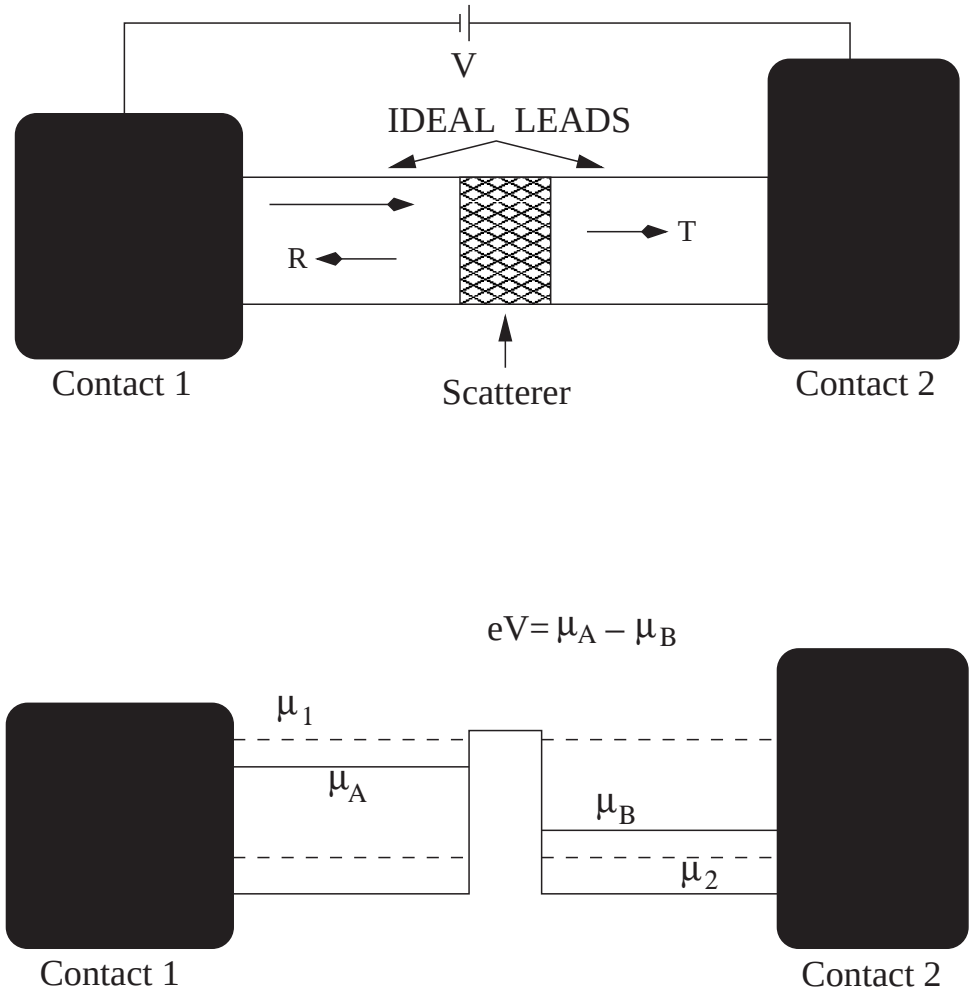

Figure I.2: A conductor with one scatterer having a transmission probability of T is connected between two large contacts through two leads, and this system can be reduced to the barrier problem.

It is important to note that with a suitable combination of the density of states and the Fermi velocity, no quantity related to the energy band of the electrons appear in the final expression for the conductance, G.

However, the actual case is more complicated. The conductance we have found above is not that of the ideal leads but that of the system containing the ideal leads. Considering the definition of the ballistic conductor we naturally expect that such a mesoscopic conductor has no resistance, when the transmission probability is equal to unity. However, Equation I.2 gives the non-zero value $h/2e^2$ for that case. This resistance, which is called as contact resistance, arises from the interface between conductor and the contacts which are very dissimilar materials [16]. While the current is being carried in the contacts by infinitely many transverse modes, inside the conductor it is carried by only a few modes. The difference between the number of modes that are carrying the current causes the resistance at the interface[17]. For $T = 1$ then, contact resistance is

$$G_c^{-1} = \frac{h}{2e^2} \approx 12.9k\Omega \qquad . \tag{I.3}$$

Consider now the situation where the wire has one scatterer with a transmission probability T as shown in Figure I.2. We have seen that for such a case, total conductance is given by Equation I.2, and therefore the total resistance is $R_{tot} = (\frac{1}{G}) = (\frac{h}{2e^2}\frac{1}{T})$. Naturally this resistance is the sum of the contact resistance, G_c^{-1}, and the scatterer resistance, G_s^{-1};

$$\frac{1}{G} = \frac{h}{2e^2}\frac{1}{T} \quad = \quad G_c^{-1} + G_s^{-1} \qquad ,$$

Consequently, scatterer conductance becomes,

$$G_s = \frac{2e^2}{h}\frac{T}{1-T} \quad = \quad \frac{2e^2}{h}\frac{T}{R} \quad . \tag{I.4}$$

This formula is valid for single-channel case and known as Landauer formula. This is the original equation derived by Landauer[4]. However, in applications Equation I.2 is used since we are interested in the total conductance.

I.1.2 The Multi-Channel Case

For the single-channel case we have seen that only one 1D subband (mode, channel) is populated at the Fermi energy. However, for real mesoscopic devices where 2D or 3D leads are connected to the scattering region, the transverse excitation of the electrons in the leads have to be taken into account. In this case, the conduction takes place over all transverse excitation modes that are populated. This situation is similar to conduction over wires connected in parallel and for this reason it is called multi-channel conduction. Büttiker[5] generalized Landauer's formula to multi-channel case where the conductance is again expressed entirely in terms of the scattering probabilities.

For a proper definition of the scattering properties, consider a 2D lead in which electrons are free along the x-direction (conduction direction) and is bound along y with a potential $V(y)$. If the effective mass is m^*, the Hamiltonian to be used is

$$H = -\frac{\hbar^2}{2m^*}\left(\frac{\partial^2}{\partial x^2} + \frac{\partial^2}{\partial y^2}\right) + V(y) \quad , \tag{I.5}$$

Let $\phi(y)$ and ϵ_n be the set of transverse wavefunctions and energies respectively.

$$\left\{-\frac{\hbar^2}{2m}\frac{d^2}{dy^2}+V(y)\right\}\phi(y)=\epsilon_n\phi_n(y) \qquad (n=1,2,...). \tag{I.6}$$

Then the eigenfunctions of H are

$$\psi(x,y)=\phi_n(y)e^{ikx} \tag{I.7}$$

with energy eigenvalues

$$E=\epsilon_n+\frac{\hbar^2k^2}{2m^*} \quad . \tag{I.8}$$

As a result, many 1D subbands are formed in the lead corresponding to different transverse excitation modes. In each band the electrons are free to move along conduction axis and hence can contribute to the conduction process. However, depending on the Fermi energy, E_F, only a finite number of these subbands will be populated, as a result, only these will contribute to the conduction at zero temperature. But, at finite temperatures all bands will have a contribution. For wavefunctions at the Fermi level, we define the wavenumber

$$k_n=\sqrt{(E_F-\epsilon_n)\frac{2m^*}{\hbar^2}} \quad . \tag{I.9}$$

For occupied subbands, $E_F>\epsilon_n$, we choose to define k_n as a positive quantity. As a result, electrons can have $+k_n$ and $-k_n$ as the number. These correspond to the electrons at the Fermi level propagating to right and left respectively.

We extend the definition of Equation I.9 to unoccupied subbands, $E_F<\epsilon_n$, and define k_n as $i\kappa_n$ where κ_n is a positive quantity. In this case, the wavenumber k_n describes a wave decreasing to the right and $-k_n$ describes a wave decreasing to the left. These are evanescent modes having no contribution

to the conduction process. However, they have to be taken into account for a correct solution of wavefunctions when scattering region is included.

Consider a general solution for the wavefunction of an electron at the Fermi level. The wavefunction on the leads to the left and to the right of the scattering regions can be written as

$$\psi_{left} = \sum_n \frac{1}{\sqrt{|k_n|}} \phi_n(y)(a_n e^{ik_n x} + c_n e^{-ik_n x}) \quad , \tag{I.10}$$

$$\psi_{right} = \sum_n \frac{1}{\sqrt{|k_n|}} \phi_n(y)(d_n e^{ik_n x} + b_n e^{-ik_n x}) \quad . \tag{I.11}$$

Here a_n and b_n are incident wave's amplitudes (we set $a_n = b_n = 0$ for evanescent modes) and c_n and d_n are amplitudes of outgoing waves. Using the well-known expression for particle current density

$$\overrightarrow{J} = \frac{\hbar}{2m^* i}(\psi^* \overrightarrow{\nabla} \psi - \overrightarrow{\nabla} \psi^* \psi) \quad , \tag{I.12}$$

the total particle current carried along x-axis is,

$$I = \int_{-\infty}^{\infty} J_x(y) \quad dy \quad . \tag{I.13}$$

Since the particle current is conserved, we get

$$I = (-e)\frac{\hbar}{m^*} \sum_n{}' |a_n|^2 - |c_n|^2 = (-e)\frac{\hbar}{m^*} \sum_n{}' |d_n|^2 - |b_n|^2 \quad , \tag{I.14}$$

where prime denotes summation over propagating modes. We would like to write this equation as

$$\sum_n{}' |a_n|^2 + |b_n|^2 = \sum_n{}' |c_n|^2 + |d_n|^2 \quad , \tag{I.15}$$

which implies that the total incident current is equal to the total outgoing current.

The scattering amplitudes of this system is defined as the coefficients of the linear dependence of outgoing waves' amplitudes to that of incident waves'

$$c_n = \sum_m{}' r_{nm} a_m + \sum_m{}' t'_{nm} b_m \qquad , \tag{I.16}$$

$$d_n = \sum_m{}' t_{nm} a_m + \sum_m{}' r'_{nm} b_m \qquad . \tag{I.17}$$

Current conservation implies unitary of the scattering matrix

$$S = \begin{bmatrix} r & t' \\ t & r' \end{bmatrix} \qquad . \tag{I.18}$$

Consider a wave incident in mode n from the left lead

$$a_m = \delta_{nm}, \quad b_m = 0 \qquad \Rightarrow \qquad c_m = r_{mn}, \quad d_m = t_{mn} \tag{I.19}$$

Then, by using current conservation we get

$$1 = \sum_m{}' |r_{mn}|^2 + |t_{mn}|^2 \qquad . \tag{I.20}$$

This equation enables us to interpret $T_{mn} = T_{m \leftarrow n} = |t_{mn}|^2$ as the transmission probability from mode n (on left) to mode m (on right). Similarly, $R_{mn} = R_{m \leftarrow n} = |r_{mn}|^2$, is the reflection probability from mode n (on left) to mode m (on right). The total transmission and reflection probabilities for mode n are

$$T_n = \sum_m{}' T_{mn} \qquad , \qquad R_n = \sum_m{}' R_{mn}$$

respectively. Finally, the current conservation implies that the electron is either reflected or absorbed

$$T_n + R_n = 1 \qquad . \tag{I.21}$$

Considering the situation where carriers in a mode n are injected into the perfect wire only from the left-hand side (LHS) and then they are transmitted to the right-hand side (RHS) in the mode m, then the current flow from mode n and mode m is

$$I_{nm} = \frac{2e}{h} T_{mn}(\mu_1 - \mu_2) \qquad . \tag{I.22}$$

The total current from the mode n on the LHS between is now:

$$I_n = \frac{2e}{h}[\sum_m{}' T_{mn}](\mu_1 - \mu_2) = \frac{2e}{h} T_n(\mu_1 - \mu_2) \qquad . \tag{I.23}$$

Then the total current is given by

$$I_{tot} = \sum_n{}' I_n = \frac{2e}{h}[\sum_n{}' T_n](\mu_1 - \mu_2) = \frac{2e}{h} Tr(tt^+)(\mu_1 - \mu_2) \qquad . \tag{I.24}$$

Consequently, conductance can be written as

$$G = \frac{2e^2}{h}\sum_m{}' T_m = \frac{2e^2}{h}\sum_{mn}{}' T_{mn} = \frac{2e^2}{h} Tr(tt^+) \qquad . \tag{I.25}$$

This is the conductance of the whole system. Büttiker[5] has found that the conductance of only the scattering region is given by

$$G = \frac{2e^2}{h}\sum_i{}' T_i \frac{2\sum_i \upsilon_i^{-1}}{\sum_i (1 + R_i - T_i)\upsilon_i^{-1}} \qquad . \tag{I.26}$$

where υ_i is the Fermi velocity of ith subband.

Finally, the conductance quantization can be understood simply in terms of Eq. (I.26). If the contact potential is very smooth so that there is no reflection of the electrons, then all transmission coefficients of the propagating modes is equal to 1. In that case, the total conductance becomes

$$G = 2\frac{e^2}{h} N \qquad , \tag{I.27}$$

where N is the number of propagating modes. A change in the gate voltage has two related effects on the contact that it defines. First, it changes the potential of the contact region and second, it changes the transverse width of the contact. Both of these effects in turn changes the number of propagating modes (modes with subband minimum, ϵ_n, smaller than Fermi energy, E_F). This results in changes in the conductance from one integer multiple of the conductance quantum to another.

I.2 Thermoelectricity

Discovery of thermoelectric effect dates back to the beginning of the 19th century. German physicist Seebeck has noticed that when a temperature difference is applied to a symmetrical circuit composed from two dissimilar metals, called as a thermocouple, an electric current is produced in the circuit, which is called as thermoelectric current (see Fig I.3). In other words, a thermocouple is a transducer that converts a temperature difference into an emf. When current is zero, if a small temperature difference, ΔT, is applied to the thermocouple a potential difference V_{12} develops on the circuit. The *thermoelectric power* of the thermocouple is defined as

$$S = S_{12} = S_1 - S_2 = \frac{V}{\Delta T} \qquad . \tag{I.28}$$

Another phenomenon was discovered by Peltier (he was a French watchmaker turned physicist) towards mids of 19th century. In contrast to the Seebeck effect, if an electric current passes from a thermocouple, then heat is

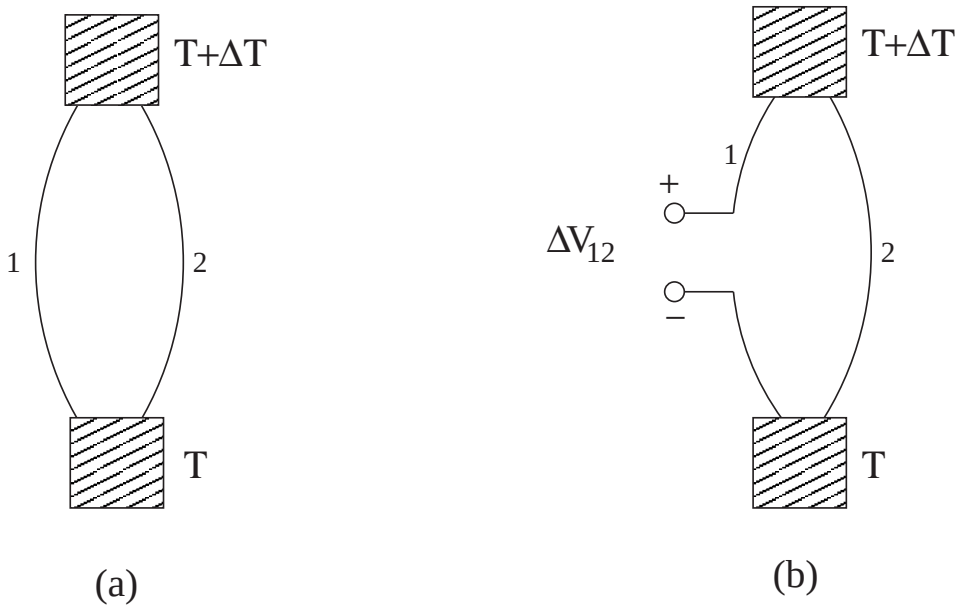

Figure I.3: *a.* Closed circuit. Basic thermoelectric circuits. If 1 and 2 are different conducting materials, a thermoelectric current will flow. *b.* Open circuit. The thermoelectric potential difference generated, ΔV_{12}, will be proportional to ΔT if $\frac{\Delta T}{T} \ll 1$.

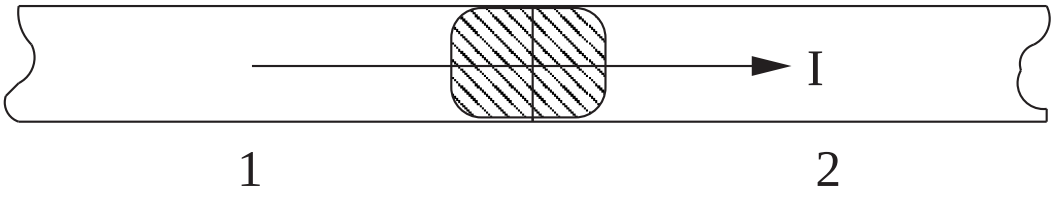

Figure I.4: Peltier heat. If an electric current I passed through the junction, heat will be evolved or absorbed, depending on the direction of I. The Peltier heat, Π_{12}, will be positive if heat is evolved at the junction in the figure, or vice versa.

liberated at one junction and absorbed at the other (see Fig I.4), depending on the direction of the current flow. This is known as the Peltier effect. The rate of heat exchange at the junction is given as,

$$\Pi_{12} = \Pi_1 - \Pi_2 \qquad \Rightarrow \qquad \dot{Q}_{emitted} = \Pi_{12} I \tag{I.29}$$

Although, this reminds the Joule heating, Peltier heating (or cooling) must be distinguished from the familiar joule heating. Since Joule heating is directly related to the electrical conductance $G = \frac{1}{R}$ of the substance, it is an entirely irreversible effect which depends on the square of the current. This means that Joule heat is always a positive quantity independent of the direction of current flow in the material. On the other hand as we mentioned above, the Peltier heat depends on both the direction and magnitude of the current flow, and may be evolved (heating up), or absorbed (cooling) depending on the relative direction of the current flow. Since, Peltier heat depends linearly in both magnitude and direction (sign) on the current flow, if a certain amount of heat evolves for a particular current, same amount of heat will be absorbed when the direction of the current is reversed. Therefore, Peltier heat is reversible.

William Thomson in 1854 noticed that there should be a thermodynamical connection between the Peltier effect and the Seebeck effect. After some calculations he found that Peltier coefficient, Π, and the Seebeck coefficient, S, of any material should be related by

$$\Pi = TS \qquad . \tag{I.30}$$

The same relation can be obtained from Onsager's reciprocity relations[18]. According to Onsager, microscopic reversibility leads to the equality of the coefficients thermal and electrical conductance. In a semiconductor or a metal, the electrons contribute to both the electrical and the thermal conduction processes, naturally there must be an interference between the two conduction which is nothing but thermoelectricity. When the electric and thermal current densities are expressed as linear functions of the driving electric field, $\overrightarrow{E}$, and the temperature gradient, $\overrightarrow{\nabla} T$ we get,

$$\overrightarrow{J_{el}} = \sigma \overrightarrow{E} + \sigma S(-\overrightarrow{\nabla} T) \qquad , \tag{I.31}$$

$$\overrightarrow{J}_{heat} = \sigma \Pi \overrightarrow{E} + \kappa'(-\overrightarrow{\nabla} T) \qquad . \tag{I.32}$$

Onsager's reciprocity relations connect the coefficients S and Π as in Equation I.30. Where, σ and κ' are electrical and thermal conductivities, respectively.

CHAPTER II

ELECTRICAL AND THERMAL TRANSPORT COEFFICIENTS IN ONE DIMENSION

II.1 Introduction

Similar to the quantization of the electrical conductance[2, 3], the thermal conductance through a quantum point contact is also quantized at integer multiples of $\frac{2}{3}\frac{\pi^2 k_B^2 T}{h}$, where factor 2 comes from spin degeneracy[24, 25]. At the late 90s, a similar quantization has been predicted for the phonon thermal conductance through a single ballistic quantum channel by Rego and Kirczenow[19]. It is also shown that the thermal conductance quantum

$$\frac{\pi^2 k_B^2 T}{3h}$$

is independent of carrier statistics[20]. The phonon thermal conductance quantization has been observed as predicted[21, 22].

In this chapter, the basic properties of the electrical and thermal conductance, and the Seebeck coefficient are investigated for a one-dimensional system. Although it is not possible to observe several quantization steps in this treatment, a few useful observations can be made.

II.2 Transport Coefficients

In the model considered here, there are two identical one-dimensional reservoirs, L and R, where electrons occupy a single parabolic band in each. The reservoirs are connected by a quasi one-dimensional wire, which allows electrons to pass from one reservoir to the other. When there is a potential and temperature difference between the reservoirs the resulting electric and entropy currents from L to R can be expressed as (including the spin degeneracy)

$$I = \frac{2}{h}\int dE(-e)\left[f(\frac{E-\mu_L}{k_BT_L}) - f(\frac{E+eV-\mu_R}{k_BT_R})\right]\mathcal{T}(E) \quad , \qquad \text{(II.1)}$$

$$I_S = \frac{2}{h}\int dE\ k_B\left[s(\frac{E-\mu_L}{k_BT_L}) - s(\frac{E+eV-\mu_R}{k_BT_R})\right]\mathcal{T}(E) \quad . \qquad \text{(II.2)}$$

Here I and I_S are the charge and entropy currents respectively; $T_{L,R}$ are the temperatures; $\mu_{L,R}$ are the chemical potentials of the reservoirs measured from the bottom of the band; V is the electrical potential difference between L and R; and $\mathcal{T}(E)$ is the transmission probability from L to R for an electron with energy E. Finally, f and s are functions for the Fermi-Dirac distribution and

entropy per electron respectively.

$$\begin{aligned} f(x) &= \frac{1}{e^x+1} \quad , \\ s(x) &= -f(x)\ln f(x) - (1-f(x))\ln(1-f(x)) \quad . \end{aligned}$$

In the linear regime considered here, the currents can be expressed in terms of the potential and temperature differences as

$$I = \frac{2e^2}{h} g_0 V^* + \frac{2(-e)k_B}{h} g_1 \Delta T \quad , \tag{II.3}$$

$$I_S = \frac{2(-e)k_B}{h} g_1 V^* + \frac{2k_B^2}{h} g_2 \Delta T \quad , \tag{II.4}$$

where $V^* = V - (\mu_L - \mu_R)/e$ is the externally applied potential difference between the reservoirs and g_n are

$$g_n = \int_{-\mu/k_BT}^{\infty} dx x^n \left(-f'(x)\right) \mathcal{T}(\mu + xk_BT) \quad , \tag{II.5}$$

where the integration is expressed in terms of $x = (E-\mu)/k_BT$. In the expressions above the variation of the chemical potential with temperature is ignored.

The transport coefficients that are directly accessible by experiment, the electrical conductance $G_{\rm el}$, the thermal conductance $G_{\rm th}$ and the Seebeck coefficient S can be expressed as

$$G_{\rm el} = \frac{2e^2}{h} g_0 \quad , \tag{II.6}$$

$$G_{\rm th} = \frac{2k_B^2}{h} T \left(g_2 - \frac{g_1^2}{g_0} \right) \quad , \tag{II.7}$$

$$S = \frac{k_B}{(-e)} \frac{g_1}{g_0} \quad . \tag{II.8}$$

In almost all cases of interest, due to the x factor in its definition, g_1 will be sufficiently small, so that the thermal conductance can be considered to be mainly proportional to g_2.

In the expression (II.5), we see that both g_0 and g_2 are proportional to some kind of an average of the transmission probability around the Fermi level. Moreover, due to the x^2 factor, the average for g_2 is over a wider energy range than that for g_0. As a result, when the transmission probability has energy dependence around the Fermi level, the thermal and electrical conductances may display different behavior as material parameters are varied. In the rest of this contribution, the behavior of these transport coefficients as a function of temperature and chemical potential are investigated.

II.3 Low Temperature Case

A special region of interest is the low temperature case, where k_BT is small compared to the typical energy scale where the transmission probability $\mathcal{T}(E)$ changes. In this case the transport coefficients can be expanded as a power series in k_BT.

$$\begin{aligned} g_0 &= \mathcal{T}(\mu) + \frac{\pi^2}{6}\mathcal{T}''(\mu)(k_BT)^2 + \cdots \quad , \\ g_1 &= \frac{\pi^2}{3}k_BT\left[\mathcal{T}'(\mu) + \frac{7\pi^2}{30}\mathcal{T}'''(\mu)(k_BT)^2 + \cdots\right] \quad , \\ g_2 &= \frac{\pi^2}{3}\left[\mathcal{T}(\mu) + \frac{7\pi^2}{10}\mathcal{T}''(\mu)(k_BT)^2 + \cdots\right] \quad . \end{aligned} \tag{II.9}$$

It can be seen that the case where temperature is zero $T = 0$ yields the same results as the case when the transmission probability is independent of

electron energy (together with the assumption $k_B T << \mu$). In these cases we have

$$G_{\rm el} = \frac{2e^2}{h}\mathcal{T} \quad , \tag{II.10}$$

$$G_{\rm th} = \frac{2\pi^2 k_B^2}{3h} T\mathcal{T} = \frac{\pi^2 k_B^2}{3e^2} T G_{\rm el} \quad , \tag{II.11}$$

$$S = 0 \quad . \tag{II.12}$$

Hence, when all electrons around the Fermi level have the same transmission probability, Wiedemann-Franz law is exactly satisfied at all temperatures. Any deviation form that law is therefore an indication of varying transmission probability around the Fermi level.

Also, the Seebeck coefficient vanishes exactly when $\mathcal{T}(E)$ is constant. On the other hand, for energy-dependent transmission probability, g_1 is proportional to the derivative of the transmission probability. Hence, the Seebeck coefficient will have large values when the transmission probability changes significantly around the Fermi level.

II.4 Intermediate Temperatures

For intermediate temperatures, we can roughly say that the energy scale over which the transmission probability $\mathcal{T}(E)$ changes, is a rough indication of the temperatures where $G_{\rm el}$ and $G_{\rm th}$ varies. Apart from this, we have to use specific models for the transmitting channel to get a good grasp of the behavior of these transport coefficients.

Below, we consider the case where the quasi one-dimensional wire con-

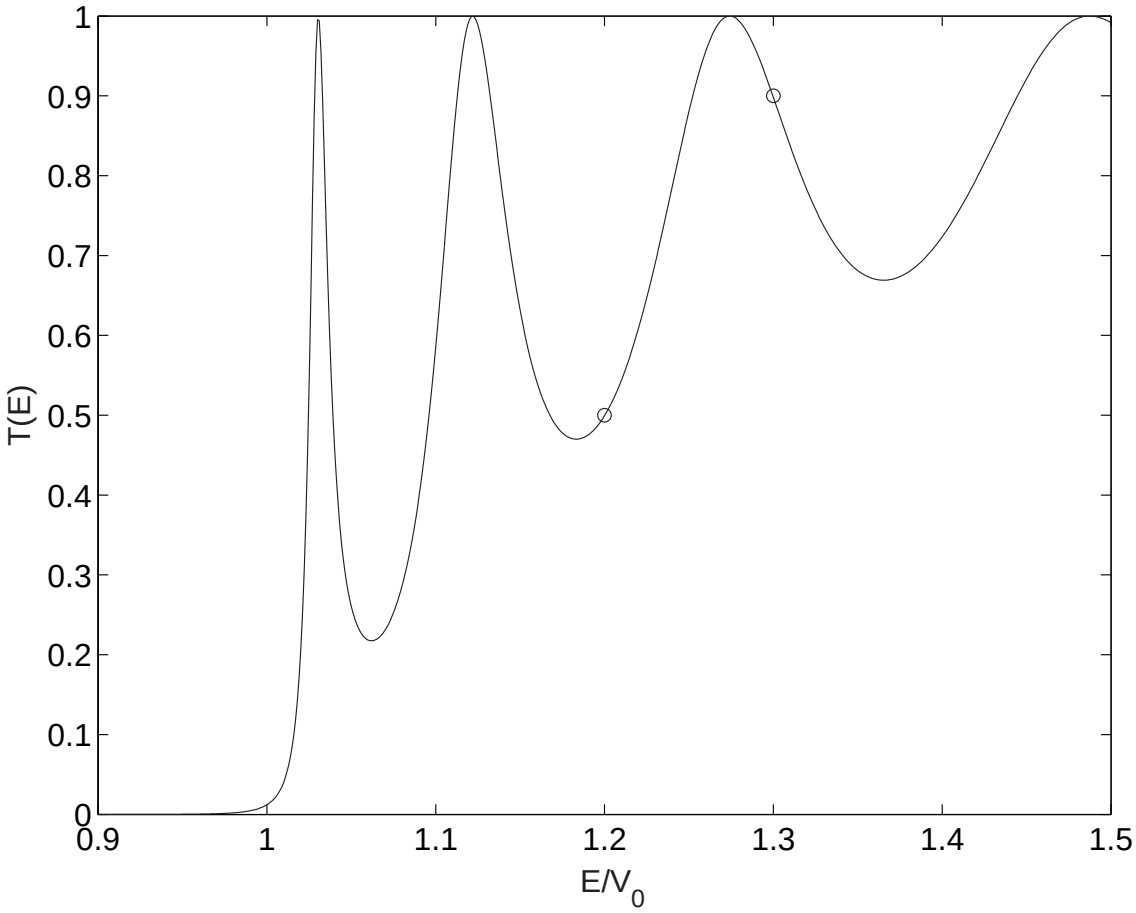

Figure II.1: Transmission probability for $\ell = 18\frac{\hbar}{\sqrt{2mV_0}}$.

necting the reservoirs contains one rectangular potential barrier with height V_0 and length ℓ. Figure II.1 shows the transmission probability for a barrier with length $\ell = 18\frac{\hbar}{\sqrt{2mV_0}}$ and Figure II.2 shows the electrical and thermal conductance as a function of temperature for this barrier.

It can be seen that when the transmission probability is close to a minimum at the Fermi level, the conductances G_{el} and G_{th} tend to increase with temperature and at a maximum of probability they tend to decrease. Apart from this, the thermal conductance has a larger variation due to the fact that the Fermi level average is over a wider range.

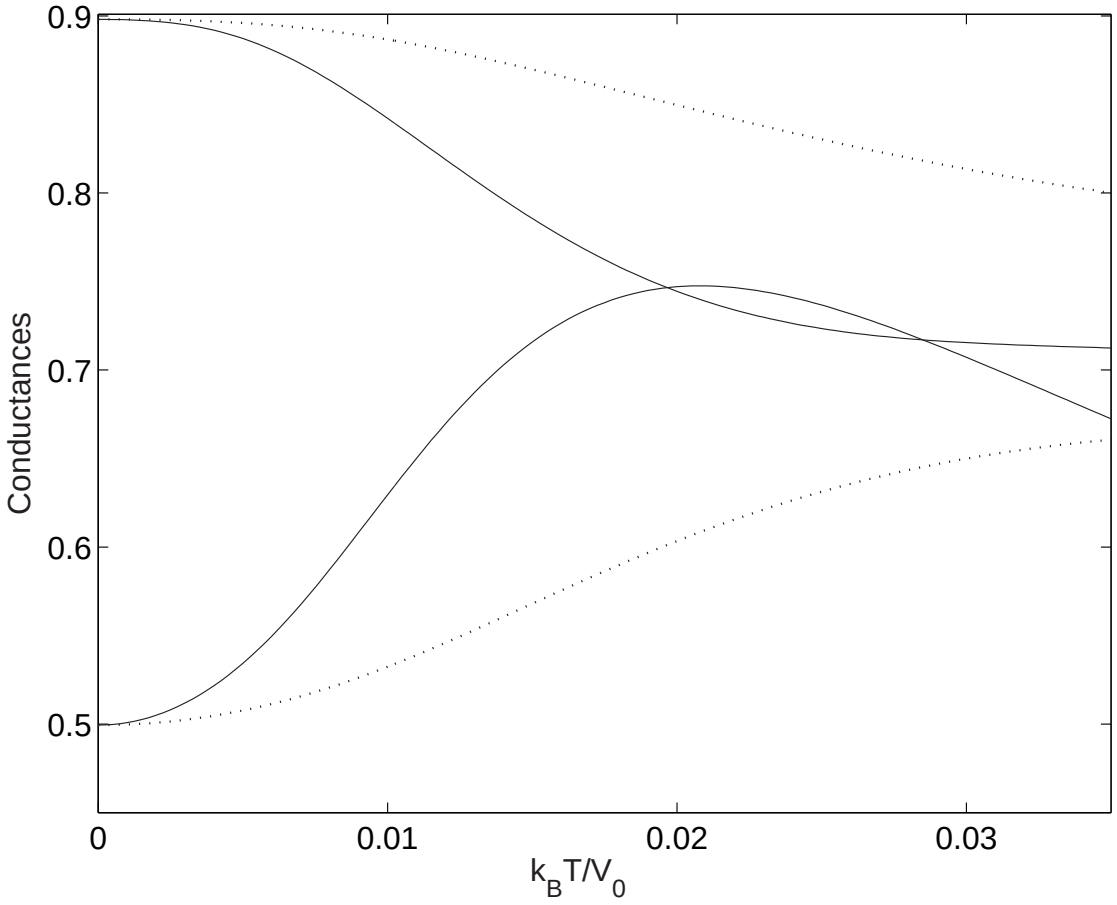

Figure II.2: Conductances as a function of temperature for two different values of chemical potential. Dotted curves are for the electrical conductance [$G_{\rm el}/(2e^2/h)$ is plotted], and the solid ones are for the thermal conductance [$G_{\rm th}/(2\pi^2 k_B^2 T/3h)$ is plotted.] The lower two curves are for $\mu = 1.2V_0$ and the upper curves are for $\mu = 1.3V_0$. Those values of μ are shown in Figure II.1 as circles.

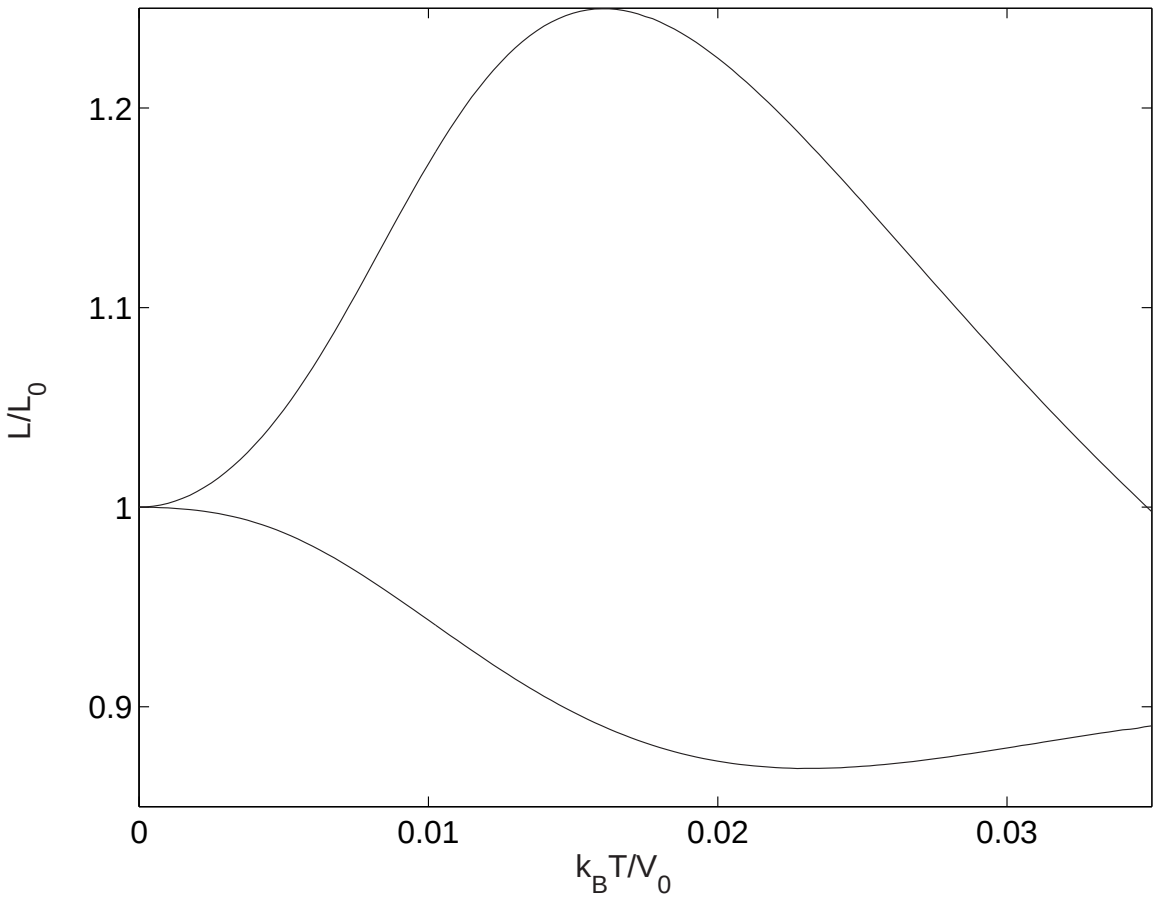

Figure II.3: Lorenz ratio divided by its ideal value for $\mu = 1.2V_0$ (upper curve) and for $\mu = 1.3V_0$ (lower curve).

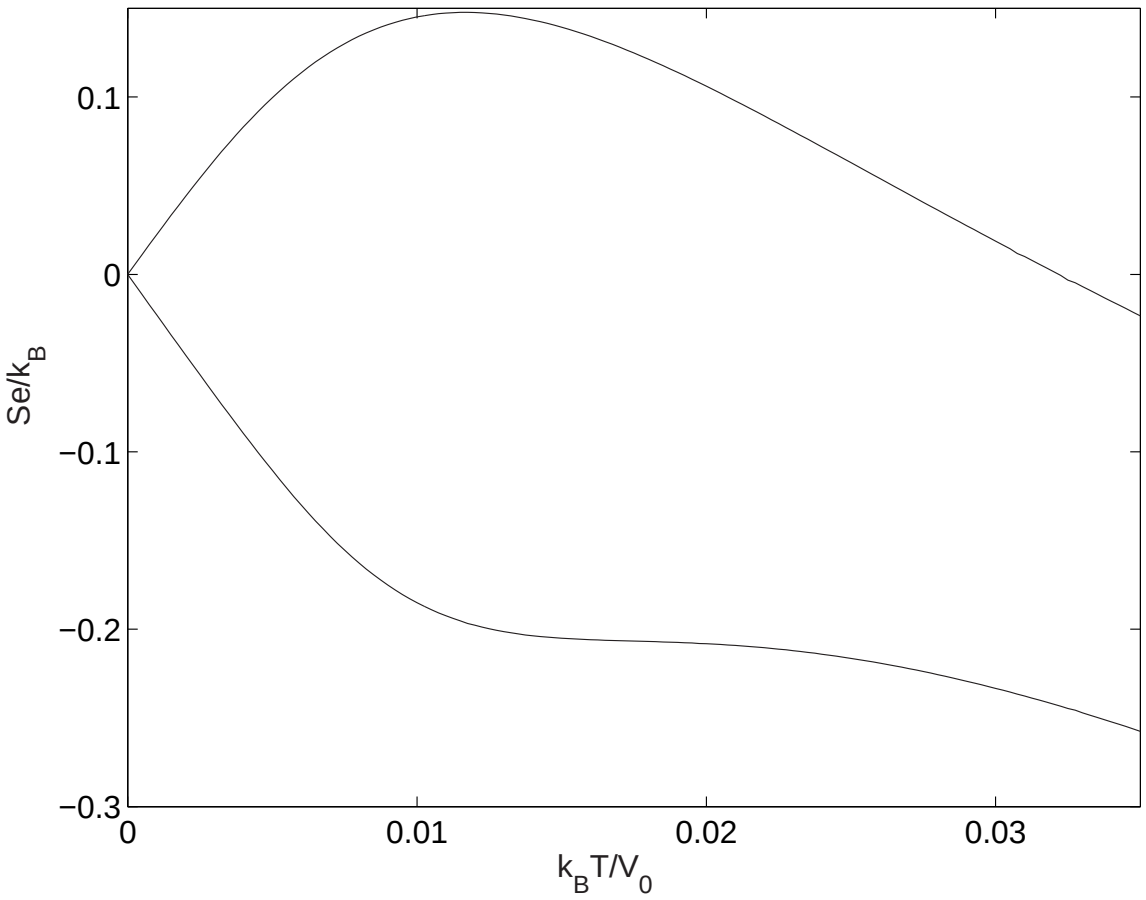

Figure II.4: The Seebeck coefficient [Se/k_B is plotted] for $\mu = 1.2V_0$ (lower curve) and for $\mu = 1.3V_0$ (upper curve).

The temperature dependence of the Lorenz ratio

$$L = \frac{G_{\text{th}}}{TG_{\text{el}}}$$

is plotted in Figure (II.3). We see that the ratio is close to the ideal value

$$L_0 = \frac{\pi^2 k_B^2}{3e^2}$$

of Wiedemann-Franz law at low temperatures, but it deviates at intermediate temperatures. It can also be seen that when the transmission probability is close to a minimum at the Fermi level, the Lorenz ratio is greater than the ideal value, and similarly around a probability maximum, ratio is smaller. This can be easily inferred from the expansions (II.9) where, as the quadratic term in temperatures are investigated g_2 varies more than g_1.

Finally, the Seebeck coefficient S is shown in Figure II.4. The behavior of S as a function of temperature is more varied and it is difficult to describe it. It is usual to see changes in sign, and it usually tend to increase with increasing temperatures. The behavior at higher temperatures are not shown.

II.5 Variation with Chemical Potential

It is useful to look at the behavior of these quantities as a function of the chemical potential, since in conductance quantization experiments it is this quantity that can be changed at will (to be more precise, gate voltage changes the energy difference between the Fermi level and the bottom of the conduction bands). In Figure II.5 the conductances are shown at a specific finite

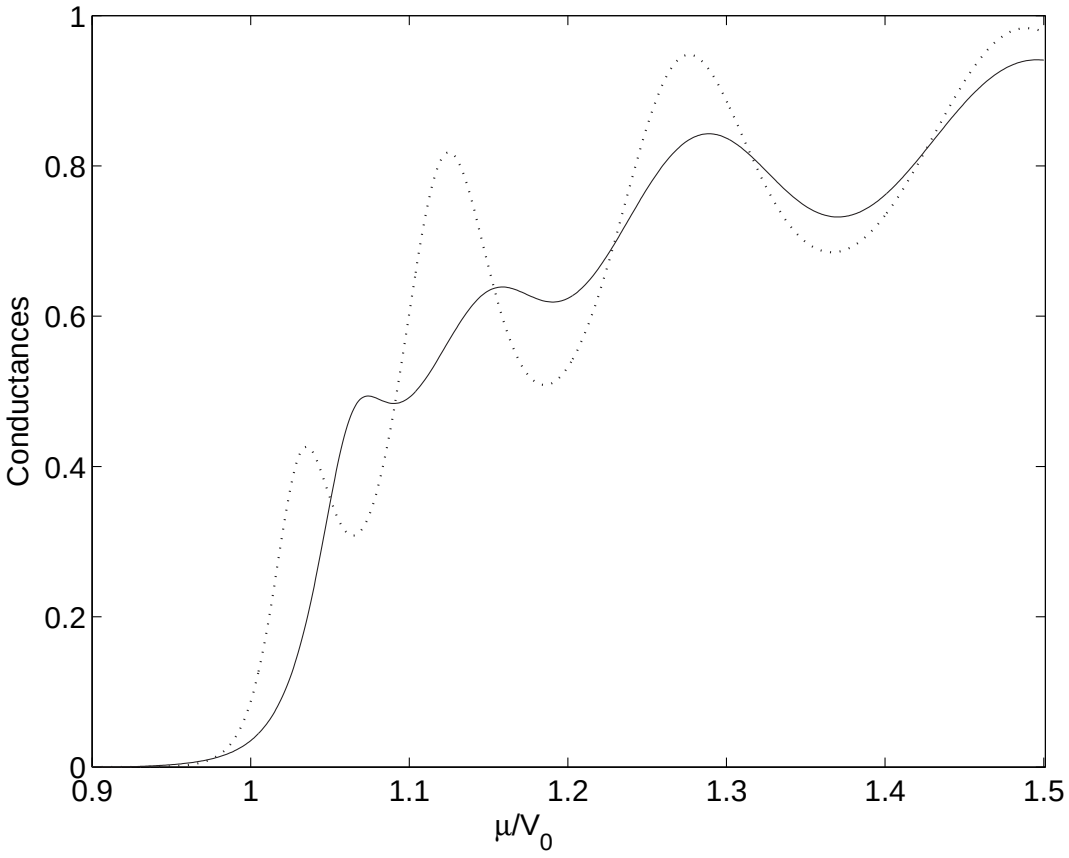

Figure II.5: The Electrical conductance (dotted curve) [$G_{\rm el}/(2e^2/h)$ is plotted] and the thermal conductance [$G_{\rm th}/(2\pi^2 k_B^2 T/3h)$ is plotted] as a function of the chemical potential μ at the temperature $k_B T = 0.01 V_0$.

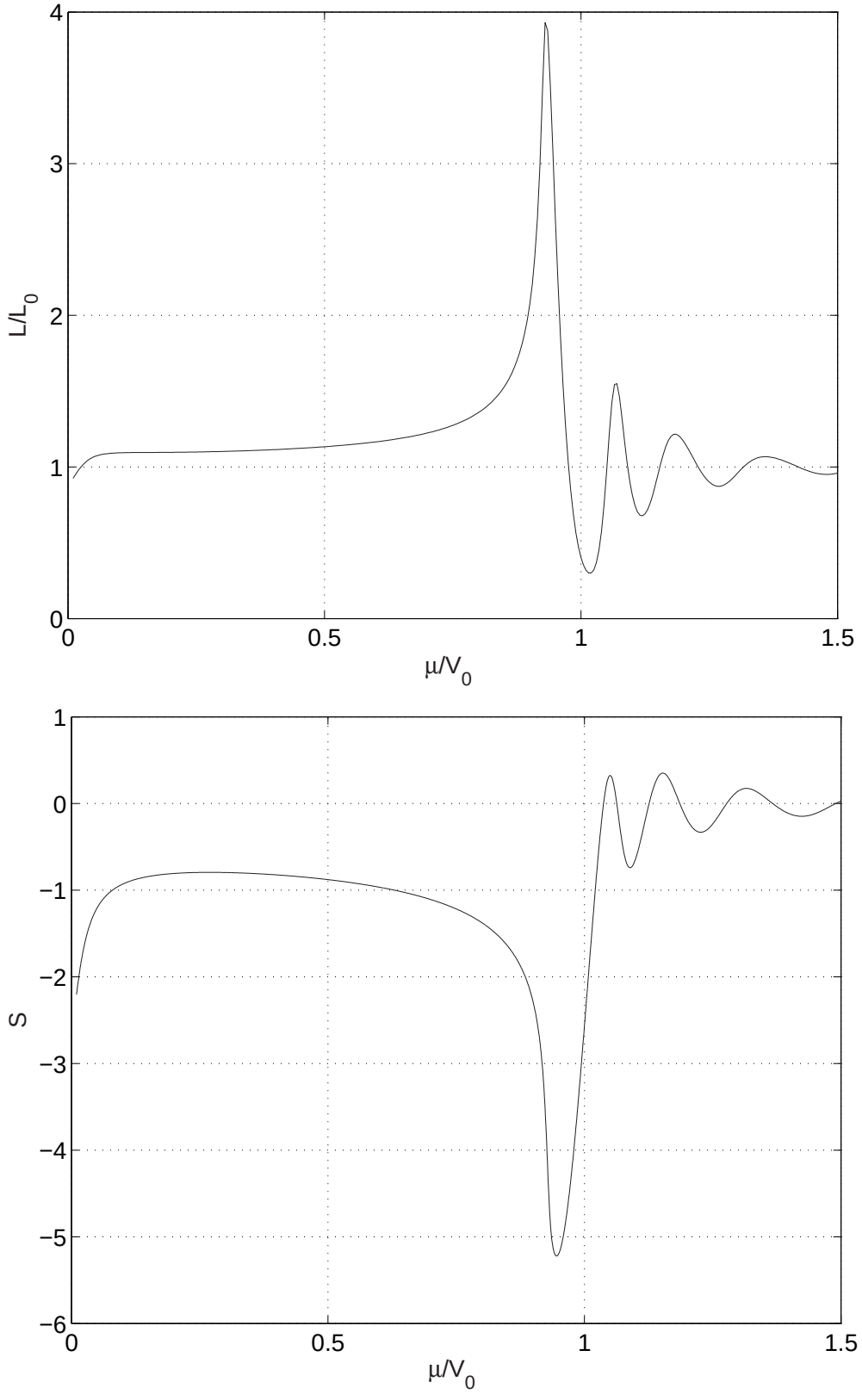

Figure II.6: Lorenz ratio divided by its ideal value (up) and the Seebeck coefficient (down) as a function of the chemical potential μ at the temperature $k_BT = 0.01V_0$.

temperature. In here, it can be seen that the electrical conductance closely resembles to the curve for the transmission probability in Figure II.1. However, the thermal conductance is more rounded. This again, is the effect of an average over a wider range at the Fermi surface. This indicates that the observation of the thermal-conductance quantization plateaus is a little bit more difficult and may require lower temperatures for observation of good quality plateaus.

Finally, the Lorenz ratio and the Seebeck coefficient is plotted in Figure II.6. A significant feature of these curves is that both quantities reach to very high values when the Fermi level is a little below than the barrier height. When it is remembered that the transmission probability has a much faster variation, from almost 0 to almost 1, in a shorter energy interval, the peaks of both of these quantities over that energy range should be understandable.

II.6 Conclusion

The behavior of the electrical and heat transport coefficients as a function of temperature and chemical potential is investigated. It is observed that the behavior of the thermal conductance closely resembles to that of electrical conductance with small differences appearing depending on the energy dependence of the transmission probability. As a function of temperature the electrical conductance is smoother while as a function of the chemical potential the thermal conductance is. This may result in less well defined plateaus for the thermal conductance in an experiment to observe quantization.

CHAPTER III

NONLINEAR SEEBECK AND PELTIER EFFECTS IN QUANTUM POINT CONTACTS

III.1 Introduction

As it is mentioned before various aspects of the ballistic electron transport across quantum point contacts are studied extensively in the past. The most striking feature of this transport is the quantization of conductance[2, 3] at integer multiples of the conductance quantum $2e^2/h$. This phenomenon is usually treated with the Landauer-Büttiker formalism[4, 5] which provides a transparent explanation for the effect. Electrons in each sub-band corresponding to the transverse modes in the contact contribute one quantum to the conductance if the sub-band is sufficiently populated. As the size of the constriction is changed by varying the negative voltage on split gates, which are

used to define the contact on a two-dimensional electron gas, the conductance changes in smooth steps from one conductance quantum into the other. It is observed that the linear Seebeck and Peltier coefficients for these structures display quantum oscillations[23, 24, 25, 26, 27] with peaks coincident with the conductance steps.

Nonlinear transport in these systems has also been studied extensively both theoretically[29, 28, 30, 31, 32, 33, 34] and experimentally[35, 36]. Since Onsager's reciprocity relations connecting the Seebeck and Peltier transport coefficients loose its meaning in this regime, these two effects show distinctively different behavior. New peaks appear in the differential Peltier coefficient as the driving voltage is increased[33, 34], while the thermopower does not change much even for very large temperature differences[36].

A major theoretical difficulty in the nonlinear regime is, due to the small size of these systems, finite voltage differences create large changes in the distribution of electrons around the contact. As a result, more involved calculations are necessary for describing the electron transport[37]. However, it is of some interest to analyze the nonlinear transport properties without taking such changes into account. Our purpose in this part is to investigate the nonlinearities in the Seebeck and Peltier effects, assuming that the contact potential is not changed apart from the uniform shift caused by the gate voltage. In the following section, the charge and heat currents are expanded as a series in powers of the potential and temperature differences. Appropriate expansions for the Seebeck and Peltier phenomena are obtained and the series

coefficients are investigated in sections III and IV, respectively. Finally, the results are summarized and discussed.

III.2 Model

In the following we consider two electron gases connected by a quantum point contact. The chemical potentials μ_L and μ_R and the temperatures θ_L and θ_R of the left (L) and right (R) reservoirs are the parameters that define the whole system and in principle all of these can be controlled experimentally. The difference between the chemical potentials, $\Delta\mu = \mu_L - \mu_R$, is equal to $(-e)V$ where V is interpreted as the electrical potential difference between L and R. A difference in temperatures $\Delta\theta = \theta_L - \theta_R$ as well as a potential difference cause electron transport which can carry both charge and heat across the contact. The average currents on the contact are completely determined by the sum

$$T(E) = \sum_n T_n(E) \quad ,$$

where $T_n(E)$ is the transmission probability of an electron with energy E incident from the nth mode. The charge and entropy currents from L to R can then be expressed as[38]

$$I = 2\frac{(-e)}{h}\int_{-\infty}^{\infty} dE(f(x_L) - f(x_R))T(E) \quad , \tag{III.1}$$

$$I_S = 2\frac{k_B}{h}\int_{-\infty}^{\infty} dE(s(x_L) - s(x_R))T(E) \quad , \tag{III.2}$$

where

$$f(x) = \frac{1}{1+e^x} \quad , \tag{III.3}$$

$$s(x) = -f(x)\log f(x) - (1-f(x))\log(1-f(x)), \tag{III.4}$$

$$x_{L,R} = \frac{E-\mu_{L,R}}{k_B\theta_{L,R}} \quad , \tag{III.5}$$

and the spin degeneracy factor is added for both currents. The expressions above can be used for any ballistic point contact by a suitable choice of $T(E)$ and for any values of the four independent parameters $\mu_{L,R}$ and $\theta_{L,R}$. However, it should be kept in mind that strong nonlinearities may alter the charge distribution around the contact and for this reason $T(E)$ has a dependence on these parameters as well. For simplicity we ignore this effect and use the same $T(E)$ throughout.

For the case of weak nonlinearities, it is useful to expand the currents in terms of the driving temperature and potential differences $\Delta\theta$ and V. In order to do this the variable of integration is changed from energy E to a dimensionless variable denoted by $\overline{x}$, which is defined as the arithmetic average of x_L and x_R.

$$\overline{x} = \frac{1}{2}(x_L + x_R) \quad .$$

This leads us to define average temperature and chemical potentials by

$$\overline{x} = \frac{E-\overline{\mu}}{k_B\overline{\theta}} \quad , \tag{III.6}$$

$$\overline{\theta} = \frac{2\theta_L\theta_R}{\theta_L+\theta_R} \quad , \tag{III.7}$$

$$\overline{\mu} = \frac{\theta_R\mu_L + \theta_L\mu_R}{\theta_R+\theta_L} \quad . \tag{III.8}$$

Here, $\overline{\theta}$ is the harmonic average of the temperatures of the two electron gases and $\overline{\mu}$ is an average of chemical potentials weighted by inverse temperatures. These two quantities will be considered as the fundamental parameters describing the contact. In other words all of the transport coefficients are considered as functions of these average quantities.

With these definitions the energy variable can expressed as $E = \overline{\mu} + \overline{x} k_B \overline{\theta}$ and the difference of the dimensionless x parameter is

$$\Delta x = x_L - x_R = -\frac{\Delta\mu + \overline{x} k_B \Delta\theta}{k_B \theta_A} \tag{III.9}$$

where θ_A is the arithmetic average of the temperatures on both sides of the contact

$$\theta_A = \frac{1}{2}(\theta_L + \theta_R) \quad .$$

Finally, dimensionless driving forces are defined as

$$\epsilon = \frac{\Delta\theta}{\theta_A} \quad , \tag{III.10}$$

$$\delta = \frac{\Delta\mu}{k_B \theta_A} \quad . \tag{III.11}$$

The obvious advantage of these definitions is the elimination of some terms in the power series expansion of the integrands in equations (III.1) and (III.2). We have

$$\begin{aligned} I &= 2\frac{(-e)}{h} \sum_{m=0}^{\infty} \frac{k_B \overline{\theta}}{2^{2m}(2m+1)!} \times \\ &\times \int d\overline{x}\ (\delta + \overline{x}\epsilon)^{2m+1} f^{(2m+1)}(\overline{x}) T(\overline{\mu} + \overline{x} k_B \overline{\theta}) \quad , \end{aligned} \tag{III.12}$$

$$\begin{aligned} I_S &= 2\frac{k_B}{h} \sum_{m=0}^{\infty} \frac{k_B \overline{\theta}}{2^{2m}(2m+1)!} \times \\ &\times \int d\overline{x}\ (\delta + \overline{x}\epsilon)^{2m+1} s^{(2m+1)}(\overline{x}) T(\overline{\mu} + \overline{x} k_B \overline{\theta}) \quad , \end{aligned} \tag{III.13}$$

where even order derivatives of the functions $f(x)$ and $s(x)$ have disappeared. This is the primary reason for defining the averages in Eqs. (III.7) and (III.8) in this particular way. Defining the parameters

$$f_{m,p} = f_{m,p}(\overline{\mu}, \overline{\theta}) = (-1)^m \int d\overline{x}\ \overline{x}^p f^{(m)}(\overline{x}) T(\overline{\mu} + \overline{x} k_B \overline{\theta}) \quad , \tag{III.14}$$

which are only functions of the contact parameters $\overline{\mu}$ and $\overline{\theta}$, the currents as can be expressed as

$$I = 2\frac{(-e)}{h} k_B \overline{\theta} \sum_{m=0}^{\infty} \sum_{p=0}^{2m+1} \frac{f_{2m+1,p} \epsilon^p \delta^{2m+1-p}}{2^{2m} p!(2m+1-p)!} \quad , \tag{III.15}$$

$$I_S = 2\frac{k_B}{h} k_B \overline{\theta} \sum_{m=0}^{\infty} \sum_{p=0}^{2m+1} \frac{[f_{2m+1,p+1} - 2m f_{2m,p}] \epsilon^p \delta^{2m+1-p}}{2^{2m} p!(2m+1-p)!} \quad . \tag{III.16}$$

This is the desired expansion of currents in terms of the driving forces ϵ and δ with the coefficients being functions of the average quantities $\overline{\mu}$ and $\overline{\theta}$.

One notable property of the equations (III.15) and (III.16) is that only the odd powers of the driving forces combined together appear in those expressions. This implies that if both driving forces change sign $\epsilon \to -\epsilon$ and $\delta \to -\delta$ then the electrical and heat currents change direction. Including only up to the third order terms in the expansions we have

$$\begin{aligned} I &= 2\frac{(-e)}{h} k_B \overline{\theta} \left(f_{10}\delta + f_{11}\epsilon \right. \\ &\quad \left. + \frac{1}{24}\left(f_{30}\delta^3 + 3f_{31}\delta^2\epsilon + 3f_{32}\delta\epsilon^2 + f_{33}\epsilon^3 \right) + \cdots \right) \end{aligned} \tag{III.17}$$

$$\begin{aligned} I_S &= 2\frac{k_B^2 \overline{\theta}}{h} \left(f_{11}\delta + f_{12}\epsilon + \frac{1}{24}\left((f_{31} - 2f_{20})\delta^3 + 3(f_{32} - 2f_{21})\delta^2\epsilon \right. \right. \\ &\quad \left. \left. + 3(f_{33} - 2f_{22})\delta\epsilon^2 + (f_{34} - 2f_{23})\epsilon^3 \right) + \cdots \right) \end{aligned} \tag{III.18}$$

These equations give the currents for arbitrary values of the temperature and potential differences. However, measurements are rarely carried out for ar-

bitrary $\Delta\theta$ and V. Electrical conductance and Peltier effect measurements are carried out at isothermal conditions while the thermal conductance and Seebeck effect measurements are done with zero electrical current. But, the equations above is a starting point for each particular phenomenon. In the following, only the Seebeck and Peltier effects are investigated.

III.3 Seebeck Effect

In the Seebeck effect, a temperature difference creates a potential difference across the point contact when there is no electrical current ($I = 0$). This potential difference can be expressed in dimensionless form as

$$-\delta = \sigma_1\epsilon + \sigma_3\epsilon^3 + \sigma_5\epsilon^5 + \cdots \tag{III.19}$$

where the first two coefficients are

$$\sigma_1 = \frac{f_{11}}{f_{10}} \tag{III.20}$$

$$\sigma_3 = \frac{1}{24 f_{10}}\left(f_{33} - 3f_{32}\sigma_1 + 3f_{31}\sigma_1^2 - f_{30}\sigma_1^3\right) \tag{III.21}$$

In terms of V and $\Delta\theta$ the series expansion is

$$-V = S_1\Delta\theta + S_3\Delta\theta^3 + S_5\Delta\theta^5 + \cdots \tag{III.22}$$

where

$$S_m = \frac{k_B}{(-e)}\frac{1}{\theta_A^{m-1}}\sigma_m \qquad m = 1, 3, 5, \ldots$$

Appearance of only the third order terms in Eq. (III.22) implies that when the temperatures of the two reservoirs are exchanged (in other words the sign of

$\Delta\theta$ is changed without changing θ_A and $\overline{\theta}$), the induced potential difference due to the Seebeck effect is reversed.

The nonlinear terms in Eq. (III.22) becomes significant when

$$\Delta\theta_{\text{threshold}} \sim \sqrt{\left|\frac{S_1}{S_3}\right|} \quad .$$

It is possible to get a theoretical estimate of this quantity in the small temperature limit, when $k_B\overline{\theta} \ll E_L$, where E_L is the energy range where $T(E)$ changes by one. In this case, the Taylor series expansion

$$T(\overline{\mu} + xk_B\overline{\theta}) \approx T(\overline{\mu}) + xk_B\overline{\theta}T'(\overline{\mu})$$

in Eq. (III.14) gives the following approximate expressions for σ_1 and σ_3

$$\sigma_1 \approx \frac{\pi^2}{3}\frac{T'}{T}k_B\overline{\theta} \quad , \qquad \sigma_3 \approx \frac{\pi^2}{12}\frac{T'}{T}k_B\overline{\theta} \quad .$$

The threshold level for nonlinearity is then

$$\Delta\theta_{\text{threshold}} \sim 2\theta_A = \theta_L + \theta_R \quad .$$

Since $\Delta\theta$ can never go above this level, the nonlinearities in the Seebeck effect is always small[36]. For this reason, the expansion (III.22) is appropriate for almost all nonlinear cases. For the opposite, high temperature limit, numerical calculations of the Seebeck coefficients indicates that the threshold expression given above does not change much.

As for the general behavior of S_3, we calculate it for a contact defined by the saddle potential

$$V(x,y) = -\frac{1}{2}m\omega_x^2x^2 + \frac{1}{2}m\omega_y^2y^2 \quad .$$

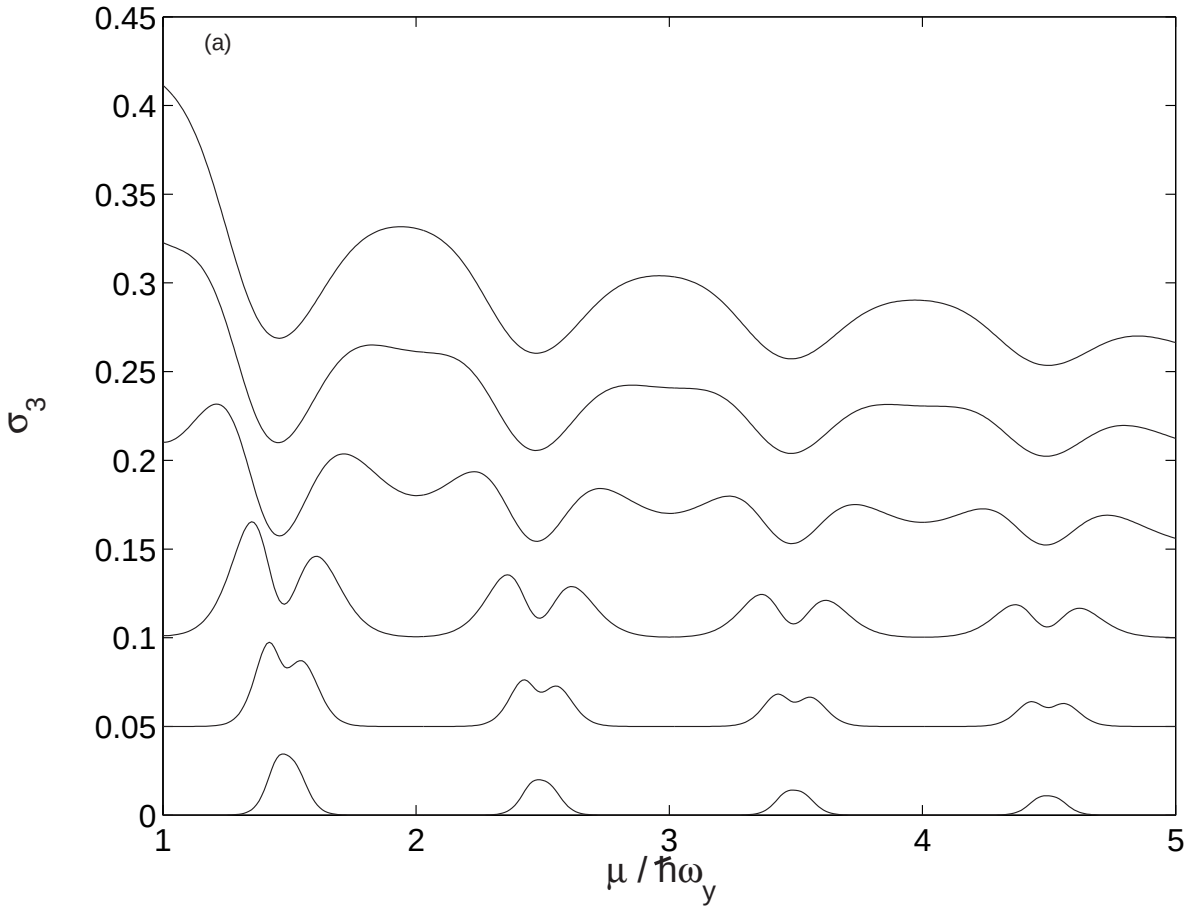

Figure III.1: The third order Seebeck coefficient, $\sigma_3 = (-e)\theta_A^2/k_B\, S_3$, is plotted as a function of average chemical potential $\overline{\mu}$ for $\omega_y/\omega_x = 6$ and $k_B\overline{\theta}/\hbar\omega_y =$ 0.01, 0.02, 0.04, 0.08, 0.105 and 0.125 (from bottom to top). Each curve is shifted by 0.05 units for clarity.

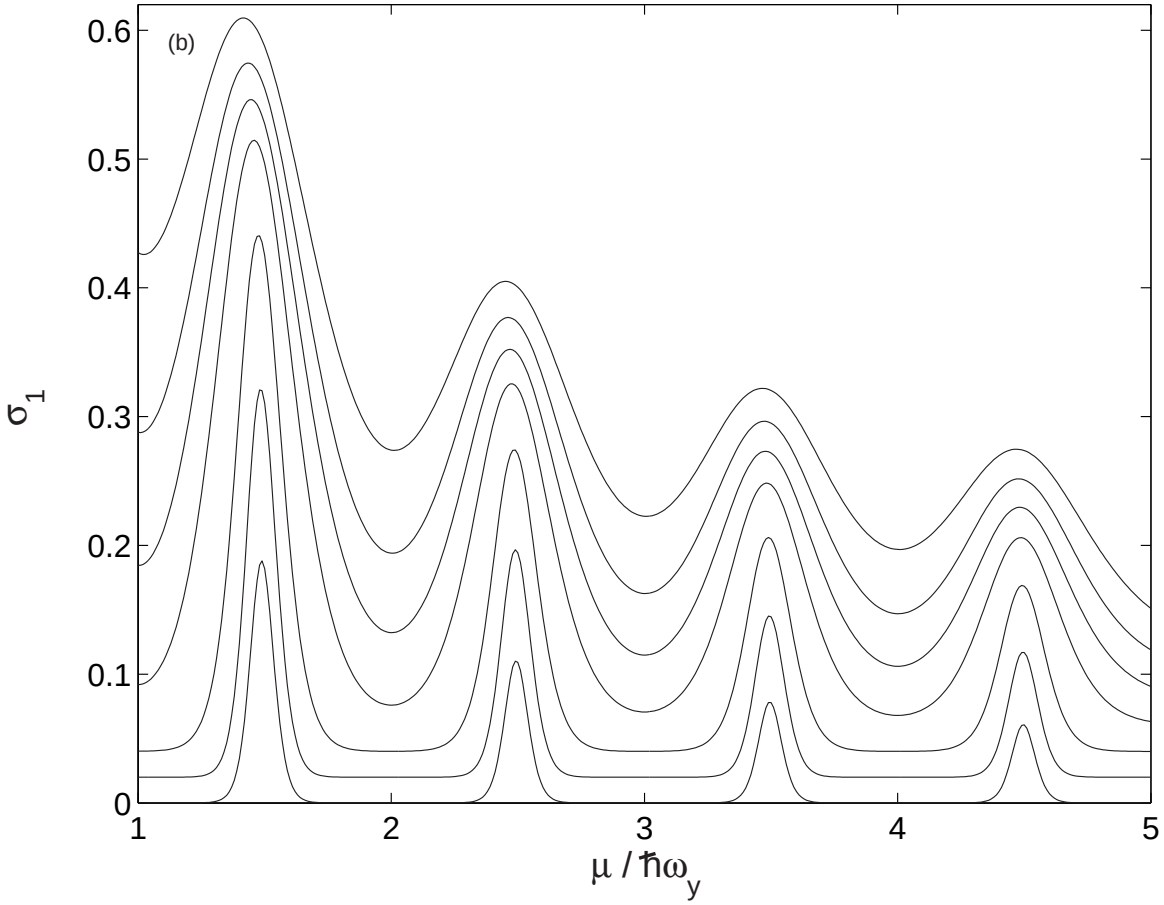

Figure III.2: For comparison the linear Seebeck coefficient, $\sigma_1 = (-e)/k_B\ S_1$, is plotted for the same set of parameters. Each curve is shifted by 0.02 units and the temperature increases from bottom to top.

For this case the energy dependent transmission probability for the nth transverse mode ($n = 0, 1, 2, \ldots$) is

$$T_n(E) = \frac{1}{1 + \exp\left(-\frac{2\pi}{\hbar\omega_x}[E - \hbar\omega_y(n + \frac{1}{2})]\right)} \quad .$$

In Fig. III.1, S_3 is plotted against $\overline{\mu}$ for this potential. At sufficiently low temperatures, third order Seebeck coefficient, S_3, has single peaks coincident with the peaks of S_1. When the temperature is increased, these peaks start to split into two. This change happens around $k_B\overline{\theta}/\hbar\omega_x \sim 0.08$. It is observed that the distance between the peaks is proportional to the temperature. For this reason, with increasing temperature the structure develops into two separate peaks. It is also observed that the widths of the peaks are also proportional to the temperature. Inevitably, when the temperature is increased further (around $k_B\overline{\theta}/\hbar\omega_y \sim 0.08$), each peak of the pair starts overlapping with the peaks of the neighboring steps. For this reason, in this high temperature regime the nonlinearity in the Seebeck effect becomes more significant away from the steps (at the plateaus of the electrical conductance). Same graphs are shown in Fig. III.3 for different values of ω_y/ω_x ratio. It can be seen that S_3 has single peaks for small values of ω_y/ω_x ratio (around $\omega_y/\omega_x \sim 1$), and peak splitting occurs for larger values of the ω_y/ω_x ratio.

In all cases it can be seen that S_3 is always negative (σ_3 is always positive) and never changes sign. It implies that the nonlinearity increases the generated Seebeck voltage further than the linear term alone suggests. Note that this feature of S_3 is not apparent from its definition, Eqn. (III.21). This appears

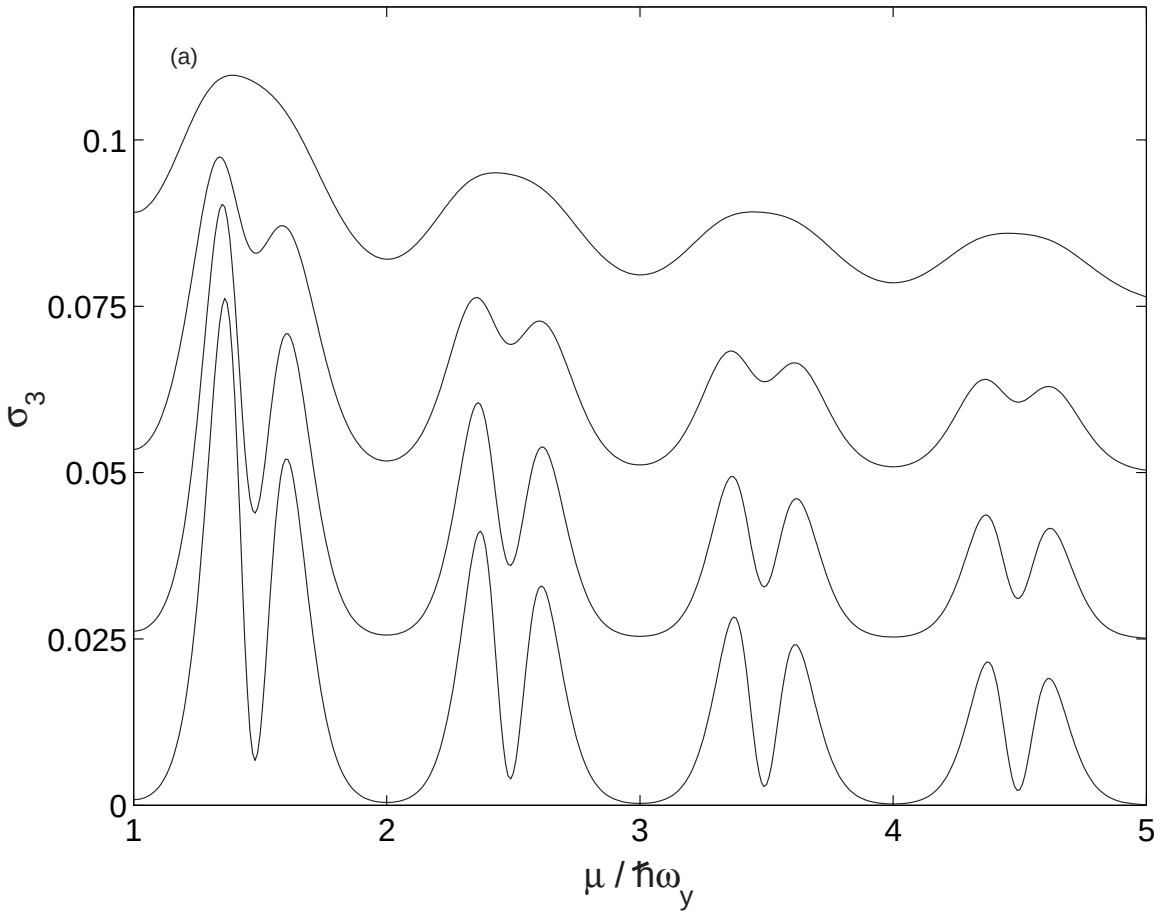

Figure III.3: The third order Seebeck coefficient, $\sigma_3 = (-e)\theta_A^2/k_B\, S_3$, is plotted as a function of average chemical potential $\overline{\mu}$ for $k_B\overline{\theta}/\hbar\omega_y = 0.04$ and $\omega_y/\omega_x =$ 1.5, 3, 6 and 12 (from top to bottom) respectively. Each plot is shifted by 0.025 units for clarity.

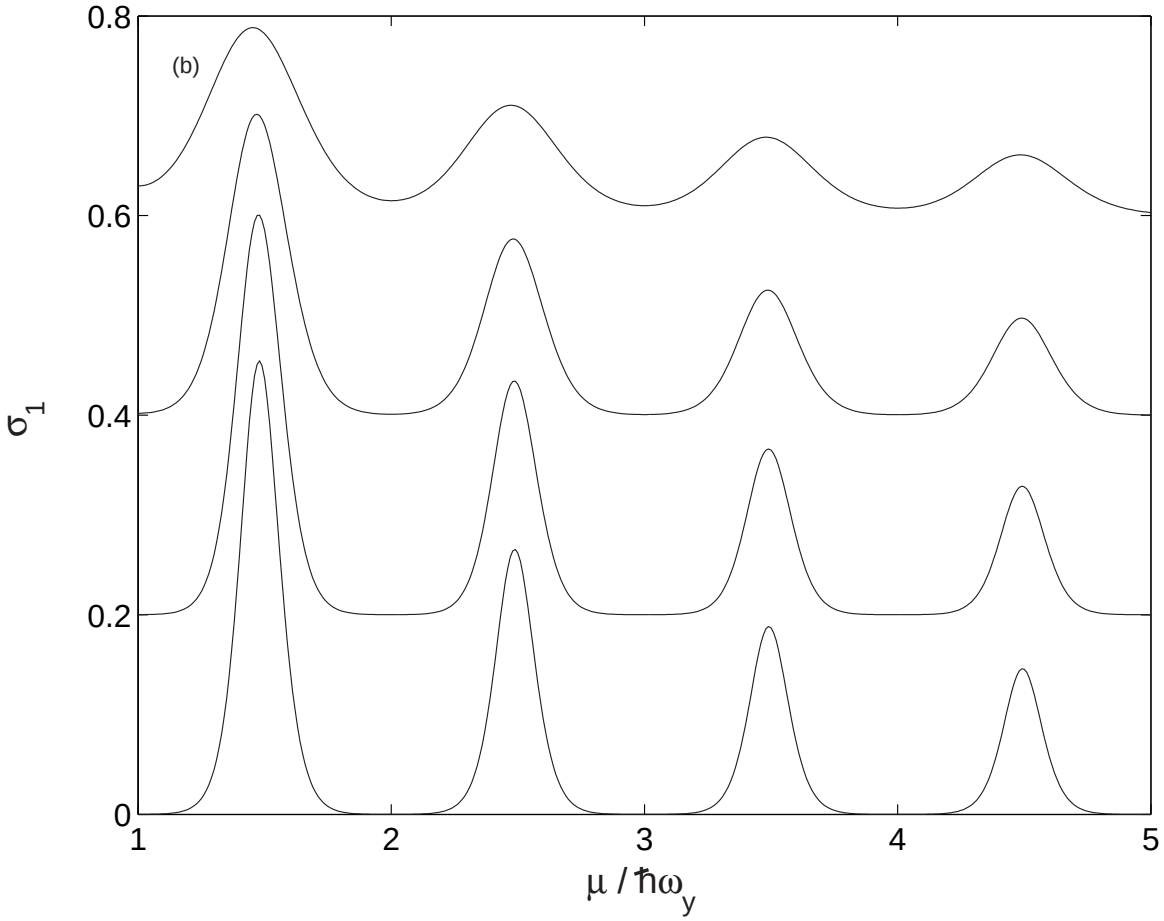

Figure III.4: For comparison, the linear Seebeck coefficient, $\sigma_1 = (-e)/k_B\, S_1$, is plotted for the same set of parameters. Each plot is shifted by 0.2 units and ω_y/ω_x ratio increases from top to bottom.

to be a model dependent feature. Especially if $T(E)$ may decrease for some energies, S_3 may display sign changes. But for the saddle potential model and for all parameter ranges investigated in this study, S_3 is found to have the same sign.

III.4 Peltier Effect

The Peltier heat is defined as the heat, $\dot{Q} = \theta I_S$, carried by the charge current I at isothermal conditions ($\theta_L = \theta_R = \theta$). The expansion of the Peltier heat and the charge current in terms of the δ parameter is

$$\dot{Q} = 2\frac{(k_B\theta)^2}{h}\left(f_{11}\delta + \frac{1}{24}(f_{31} - 2f_{20})\delta^3 + \frac{1}{1920}(f_{51} - 4f_{40})\delta^5 + \cdots\right) \quad , \text{(III.23)}$$

$$I = 2\frac{(-e)}{h}\left(f_{10}\delta + \frac{1}{24}f_{30}\delta^3 + \frac{1}{1920}f_{50}\delta^5 + \cdots\right). \quad \text{(III.24)}$$

Both of these expressions can be used to expand $\dot{Q}$ as a power series of the current I

$$\dot{Q} = \Pi_1 I + \Pi_3 I^3 + \Pi_5 I^5 + \cdots \quad , \quad \text{(III.25)}$$

where the first two terms of the expansion are

$$\Pi_1 = \frac{k_B\theta}{(-e)}\frac{f_{11}}{f_{10}} \quad , \quad \text{(III.26)}$$

$$\Pi_3 = \frac{h^2}{(-e)^3 k_B\theta}\frac{f_{10}(f_{31} - 2f_{20}) - f_{11}f_{30}}{96 f_{10}^4} \quad , \quad \text{(III.27)}$$

The appearance of only the odd powers of the current in the expansion of $\dot{Q}$ signifies the reversible character of the Peltier heat. The coefficient Π_1 is for the linear Peltier effect, which is related to S_1 through the Thomson-Onsager relation by $\Pi_1 = \theta S_1$.

The plots of Π_3 are shown in Fig. III.5 and III.6 for the saddle potential model as a function of $\overline{\mu}$ for different values of parameters $k_B\overline{\theta}/\hbar\omega_y$ and ω_y/ω_x, respectively. For low temperatures, Π_3 is non-zero only around the steps of the conductance. But, in contrast to S_3, it displays a change of sign for all parameter values. In particular Π_3 has opposite sign at the peaks of $\Pi_1 = \theta S$. This behavior is an indication of the peak splitting[33, 34] behavior of the Peltier coefficient under nonlinear currents. In other words, with nonlinear currents, the Peltier heat decreases at the peaks of the linear Peltier coefficient, but increases at the foothills of these peaks. Similar to S_3, Π_3 is extremely small at the plateaus of the conductance for small temperatures, but when the temperature is higher (comparable to $\hbar\omega_y$) it also becomes significant at the plateau region. Finally, Π_3 is significant only around the first few steps. At higher steps, it is observed that the peak heights are inversely proportional to the cube of $T(\overline{\mu})$.

To estimate the threshold level for nonlinearity, we use the following approximations valid in small temperature limit

$$f_{31} - 2f_{20} = \frac{1}{3}\pi^2(k_B\overline{\theta})^3 T'''$$

and

$$f_{11} = (k_B\overline{\theta})T'\frac{\pi^2}{3}$$

in Eq. (III.23). Therefore, the nonlinearity sets in when the driving potential difference is of the order of

$$eV_{\text{threshold}} \sim E_L \quad .$$

Since it is possible that the driving potential difference on the contact can easily exceed this threshold level, in these highly nonlinear cases it will not be reasonable to use only a few terms of the expansion in Eq. (III.25). However, for weakly nonlinear cases, the expansion above might be useful.

III.4.1 High-order nonlinearity in Peltier effect at small temperatures

As it was discussed above, highly nonlinear cases cannot be treated appropriately by the power series expansion discussed here. For this case, we need to have a better method for evaluating the heat and charge currents passing through the contact. We consider only the isothermal case appropriate for the Peltier effect. The charge and entropy currents for this case can be expressed as

$$I = 2\frac{(-e)}{h}\int_{-\infty}^{\infty} dx(-f'(x))[A(\mu_L + xk_B\theta) - A(\mu_R + xk_B\theta)] \quad \text{(III.28)}$$

$$I_S = 2\frac{k_B}{h}\int_{-\infty}^{\infty} dx(-xf'(x))[A(\mu_L + xk_B\theta) - A(\mu_R + xk_B\theta)] \quad \text{(III.29)}$$

where $A(E)$ is the energy integral of $T(E)$,

$$A(E) = \int_{-\infty}^{E} T(E)dE \quad .$$

Assuming small temperatures ($k_B\theta \ll E_L$), the integrands can be expanded as

$$A(\mu + xk_B\theta) \approx A(\mu) + xk_B\theta T(\mu)$$

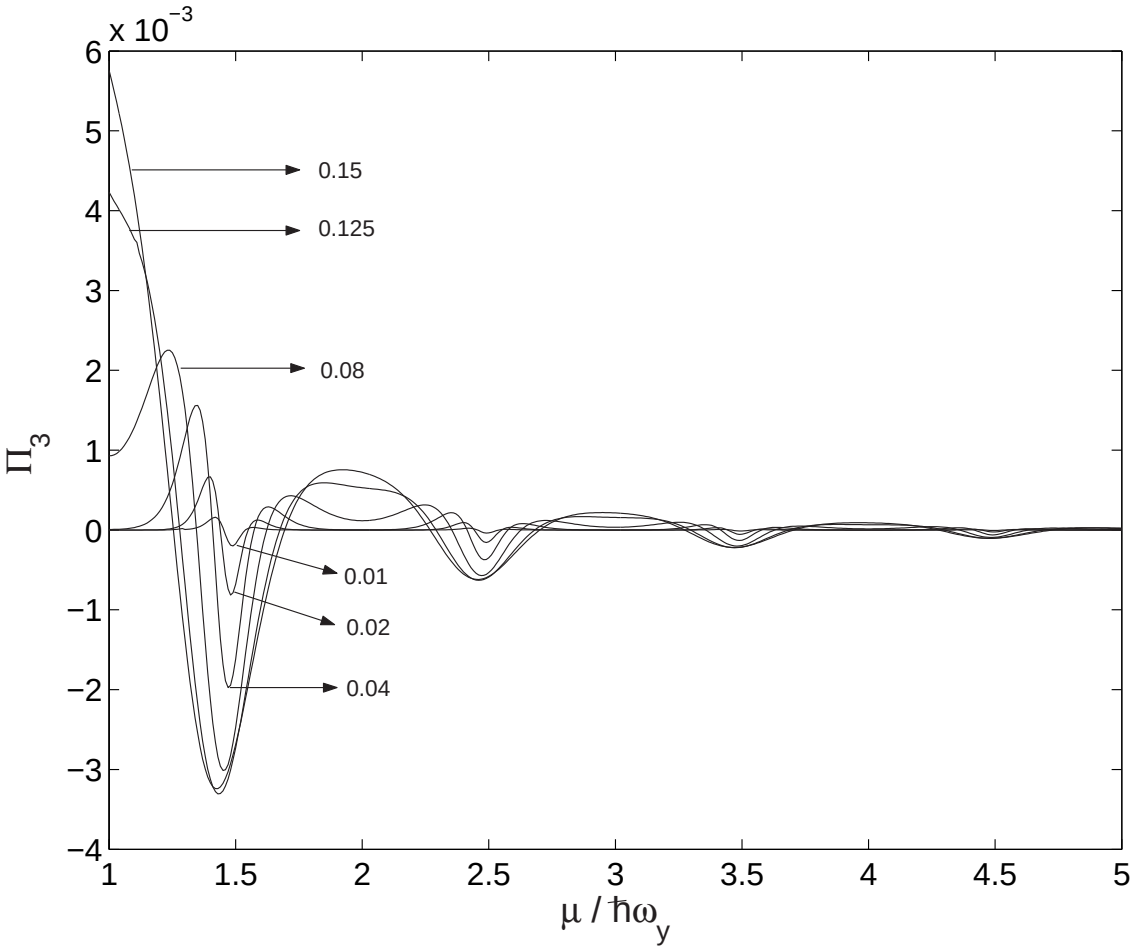

Figure III.5: The third-order Peltier coefficient Π_3 (in arbitrary units) is plotted as a function of average chemical potential $\overline{\mu}$ for $\omega_y/\omega_x = 6$ and different values of temperatures ($k_B\overline{\theta}/\hbar\omega_y$ values are indicated in the figure).
1cm

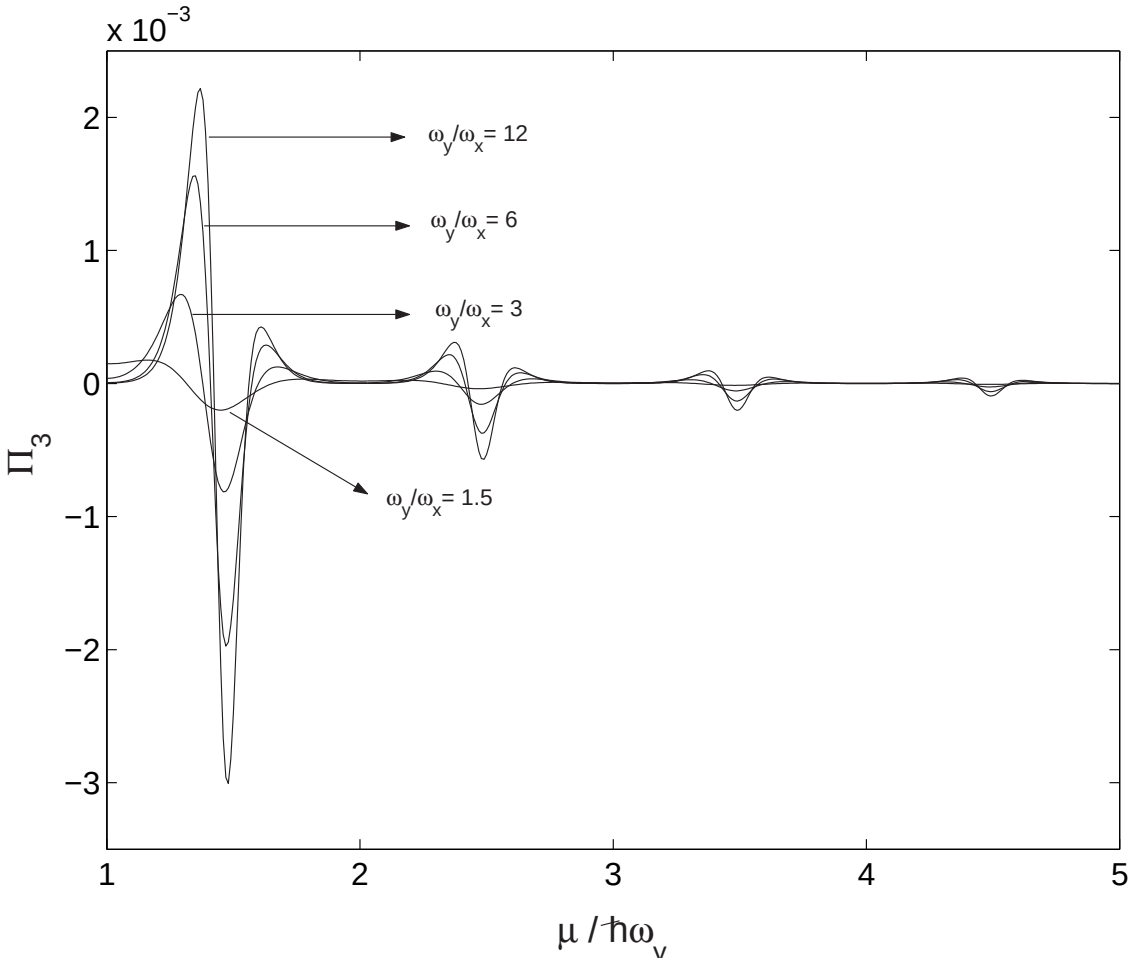

Figure III.6: The third order Peltier coefficient Π_3 is plotted as a function of average chemical potential $\overline{\mu}$ for $k_B\overline{\theta}/\hbar\omega_y = 0.04$ and different values of ω_y/ω_x whose values are indicated in the figure.

and evaluate the integrals. Keeping only the lowest order terms the currents can be expressed as

$$I = 2\frac{(-e)}{h}(A(\mu_L) - A(\mu_R)) \quad , \tag{III.30}$$

$$\dot{Q} = \frac{2\pi^2}{3h}(k_B\theta)^2(T(\mu_L) - T(\mu_R)) \quad . \tag{III.31}$$

As was discussed by Bogachek *et al.*[33, 34], the differential Peltier coefficient can be expressed as (assuming constant $\overline{\mu}$)

$$\Pi_d = \left(\frac{\partial\dot{Q}}{\partial I}\right)_{\overline{\mu}} = \frac{\pi^2(k_B\theta)^2}{3(-e)}\frac{T'(\mu_L) + T'(\mu_R)}{T(\mu_L) + T(\mu_R)} \quad .$$

The peak splitting effect of the nonlinearity can be seen from this expression. When the potential difference across the contact is less than E_L, the individual peaks of $T'(\mu_L)$ and $T'(\mu_R)$ will join in a single peak observed in the linear Peltier effect. However, if the potential difference is more than E_L, the contribution of these two terms can be distinguished since they will form two separate peaks. The distance between the peaks, then, will be proportional to the applied potential difference.

III.5 Conclusions

The expansions of the charge and entropy currents as a power series in temperature and potential differences are obtained, assuming that the transmission probabilities are unchanged by the nonlinearities. The main advantage of this particular expansion is, through a different definition of average chemical potential, $\overline{\mu}$, and temperature, $\overline{\theta}$, some particular terms disappear from the

expressions. The Seebeck and Peltier effects are investigated as special cases and it is found that the lowest order nonlinearities are of third order in both cases. As a result, ignoring the inconvenience caused by experimental difficulty in fixing $\overline{\mu}$ and $\overline{\theta}$, these coefficients can be measured by measuring the third harmonic response of the system for an AC signal.

In the case of the Seebeck effect S_3, is found to have the same sign as S_1. Although at low temperatures S_3 is found to be simply proportional to S_1, its peaks split into two at high temperatures. If $k_B\overline{\theta}$ is comparable to the energy difference between the successive sub-bands, these peaks may join with the peaks of the neighboring steps, creating an unusual appearance where S_3 has maxima at the plateaus of the conductance and minima at the steps. In all cases, it is found that the nonlinear signal is small compared to the linear one.

For the case of the Peltier effect Π_3, changes sign as the gate voltage is changed for all parameter values. The main shortcoming of the expansion developed here is that in this case the potential difference driving the current may be chosen above the threshold level for nonlinearity. In such a case, the expansion is useless as more and more terms have to be added up to obtain the correct response. In the small temperature limit, an alternative expression has been developed for the differential Peltier coefficient that is also valid for highly nonlinear cases.

CHAPTER IV

HALF STEPS IN THE LINEAR THERMAL CONDUCTANCE OF QUANTUM POINT CONTACTS

IV.1 Introduction

A large number of studies are conducted on the ballistic transport of electrons across quantum point contacts defined by the split-gate techniques on (Al,Ga)As heterostructures. An interesting feature of this transport is the quantization of the electrical conductance[39, 40] in multiples of the conductance quantum $2e^2/h$. This phenomenon is usually treated with the Landauer-Büttiker formalism[4, 5] which has a transparent explanation for the quantization. For each transverse mode in the contact, there is in effect a one-dimensional energy sub-band corresponding to that mode within the contact region. When a sub-band minimum is sufficiently below the Fermi level, the

electrons in that band contribute one quantum $2e^2/h$ to the electrical conductance for adiabatically varying contact potentials, where the factor 2 comes from spin degeneracy. As the voltage on the split gates is varied, the electrical conductance defines smooth plateaus, occasionally changing from one plateau into the other in smooth steps whenever a sub-band starts to be (un)occupied.

The thermal conductance is also quantized[24, 15, 42] in the same way in integer multiples of

$$K_0 = \frac{2\pi^2}{3h} k_B^2 \theta$$

where θ denotes the temperature. This quantization has exactly the same character as the electrical conductance. The plateaus and steps appear at the same gate voltages. This can simply be understood as a direct result of the Wiedemann-Franz law relating the thermal conductance, K, to the electrical conductance, G, by

$$\frac{K}{\theta G} = \frac{\pi^2 k_B^2}{3e^2} \quad ,$$

which is seen to remain valid in quantum point contacts although small violations can be observed around steps[24].

A remarkable difference between the curves of the two conductances as a function of gate voltage is the appearance of half plateaus in the thermal conductance, i.e., almost flat regions around half-integral multiples of K_0, which is first noted by van Houten *et al.*[15]. To the authors' knowledge, these additional plateaus have not yet been observed experimentally and there has been no detailed theoretical investigation about them. Similar half-plateau

structures have also been observed in the electrical conductance as a result of distinct causes. An applied magnetic field that lifts the spin degeneracy is one possible cause. Also, for the finite values of the source-drain voltage (i.e., at the non-linear regime) new plateau structure develops at the middle of the steps[43, 44, 45, 46]. These plateaus increase in width for increasing source-drain voltage and they eventually obliterate the normal quantization plateaus. However, the half plateaus in the thermal conductance can occur under zero magnetic field and in the linear regime. The purpose of this work is to analyze the half plateaus in the thermal conductance at different temperatures and contact parameters. The theory is summarized in the following section, after that the conductances are investigated for different parameter values. Finally, a physical explanation for the structure is provided.

IV.2 Theory

If both sides of a quantum point contact has different potentials and temperatures, the charge (I) and the heat ($\dot{Q}$) currents that pass through the contact can be expressed in the linear regime as[47]

$$I = 2\frac{e^2}{h}g_0 V + 2\frac{(-e)k_B}{h}g_1\Delta\theta \quad , \tag{IV.1}$$

$$\dot{Q} = 2\frac{(-e)k_B\theta}{h}g_1 V + 2\frac{k_B^2\theta}{h}g_2\Delta\theta \quad , \tag{IV.2}$$

where V is the electric potential difference, $\Delta\theta$ is the temperature difference and g_p are dimensionless quantities defined as

$$g_p = \int dx\ x^p\ (-f'(x))T(\mu + xk_B\theta) \quad , \quad (p = 0, 1, 2), \tag{IV.3}$$

where μ is the chemical potential, $f(x) = 1/(1+e^x)$ is the Fermi-Dirac distribution function and $T(E)$ is the sum of the transmission probabilities at energy E. In other words,

$$T(E) = \sum_n T_n(E)$$

where $T_n(E)$ is the transmission probability of an electron incident in mode n and at the energy E.

The electrical conductance, which is measured at isothermal conditions, and the thermal conductance, which is measured at zero electrical current ($I = 0$), are respectively given by

$$G = \frac{2e^2}{h} g_0 \quad , \tag{IV.4}$$

$$K = \frac{2k_B^2 \theta}{h} \left(g_2 - \frac{g_1^2}{g_0} \right) \quad . \tag{IV.5}$$

For calculating the conductances the saddle potential model[48] is used where the potential energy around the contact is expressed as

$$V(x,y) = V_0 - \frac{1}{2} m\omega_x^2 x^2 + \frac{1}{2} m\omega_y^2 y^2 \quad , \tag{IV.6}$$

where V_0 refers to the value of the constriction potential at the saddle point, x and y correspond to the longitudinal and transverse directions respectively, and curvatures of the potential are expressed in terms of the frequencies ω_y and ω_x. The transmission probabilities for this potential have been calculated as[49, 50]

$$T_n(E) = \left(1 + \exp\left(-\frac{2\pi}{\hbar\omega_x} (E - E_n) \right) \right)^{-1}$$

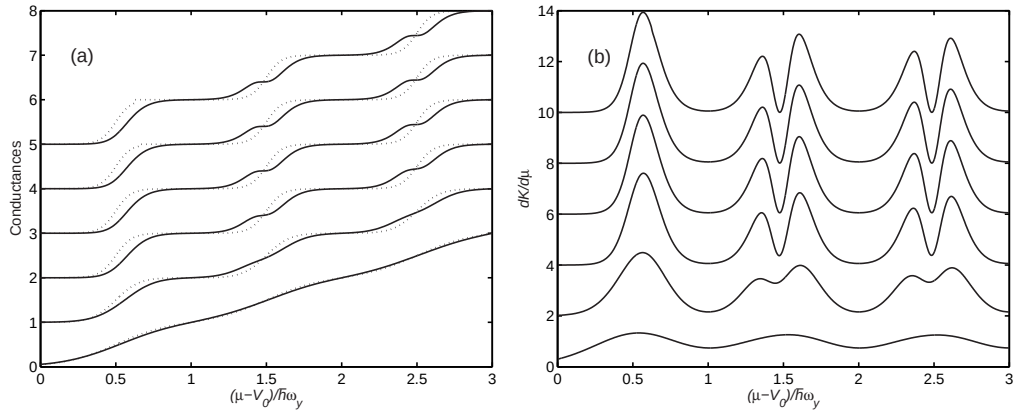

Figure IV.1: (a) The electrical conductance (dotted) in units of $2e^2/h$ and the thermal conductance (solid) in units of K_0 plotted as a function of the chemical potential. The curves are for (from bottom to top) $\omega_y/\omega_x = 1$, 3, 10, 30, 100 and 300 and $k_B\theta/\hbar\omega_y = 0.05$. Different curves are shifted vertically for the sake of clarity. (b) The derivative of the thermal conductance (in units of $K_0/\hbar\omega_y$) for the same parameter values. The ratio ω_y/ω_x increases from the bottom to the top and different curves are shifted vertically by 2 units.

for $n = 0, 1, 2, \ldots$ where $E_n = V_0 + \hbar\omega_y(n + 1/2)$. The energy scales for this problem are the sub-band separation, $E_T = \hbar\omega_y$, and the energy range for a step $E_L \approx \hbar\omega_x$. Physically, a smaller $\hbar\omega_x$ implies that the contact is longer, which results in rapid changes of tunnelling probability with electron energy.

IV.3 Results and Discussion

The electrical and thermal conductances are evaluated numerically and plotted in Fig. IV.1(a) for different values of ω_y/ω_x ratio. For large values of ω_x (short contacts) both quantities follow the same curve. But when ω_x becomes smaller (longer contacts) half plateaus in the thermal conductance start appearing excepting the first step. The development of the half plateaus can be seen more clearly in the derivative of the thermal conductance with respect to the

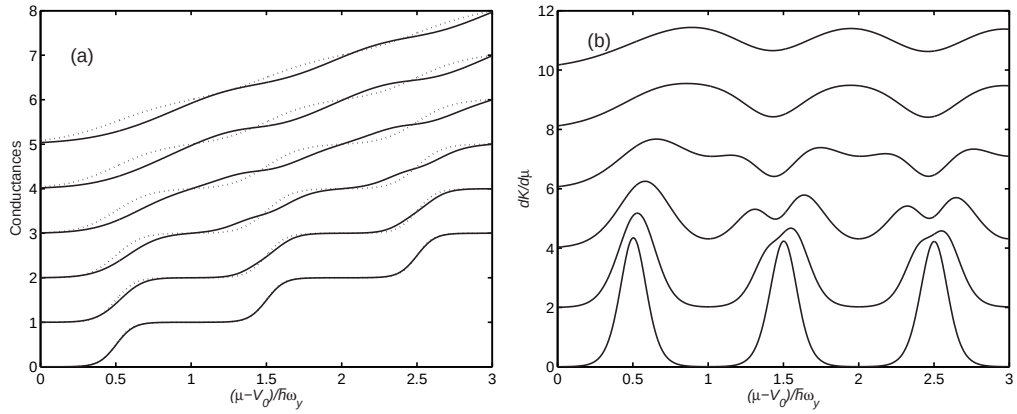

Figure IV.2: (a) The electrical conductance (dotted) in units of $2e^2/h$ and thermal conductance (solid) in units of K_0 plotted as a function of the chemical potential. The curves are obtained for (from bottom to top) $k_B\theta/\hbar\omega_y$ =0.01, 0.03, 0.06, 0.1, 0.15 and 0.2 and $\omega_y/\omega_x = 3$. Different curves are shifted vertically for the sake of clarity. (b) The derivative of the thermal conductance with respect to chemical potential (in units of $K_0/\hbar\omega_y$) for the same parameter values. Different curves are shifted vertically by 2 units for clarity and the temperature increases from the bottom to the top.

chemical potential which are shown in Fig. IV.1(b). For large values of ω_x, the derivative displays only a single peak at each step. When ω_x is decreased, the peaks first split into two indicating the development of a flatter structure. At smaller values of ω_x, the derivative in between the peaks decreases sufficiently indicating that the structure in the thermal conductance is almost flat. It can be seen from the figures that the widths of these plateaus do not change as ω_x is lowered further.

Appearance of the half-plateau structure can also be seen for increasing temperature as shown in Fig. IV.2. At low temperatures, both conductances follow the same curve as a function of the chemical potential. However, as the temperature is increased a half-plateau structure becomes apparent for

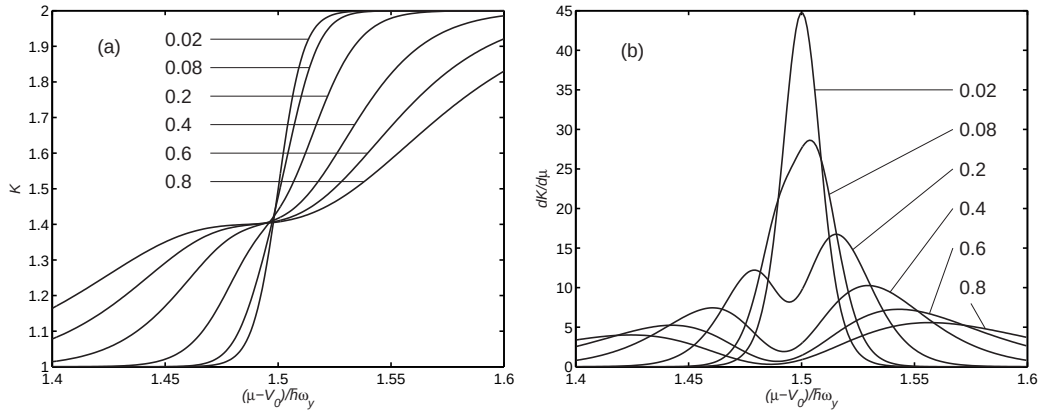

Figure IV.3: (a) The thermal conductance, K, and (b) its derivative, $\partial K/\partial\mu$, around the second step (step between $n = 1$ and $n = 2$ plateaus) for different values of $k_B\theta/\hbar\omega_x$ ratio. Values of that ratio are indicated in the graphs.

the thermal conductance. When the temperature is increased further, the half plateaus become wider and eventually wipe out the integer plateaus. It can be verified that the width of the secondary plateaus are proportional to the temperature. The obliteration of the integer plateaus become inevitable as $k_B\theta$ becomes comparable to $E_T = \hbar\omega_y$. It is interesting to observe that in this parameter range, although the integer plateaus are wiped out, half-plateau structure is still distinguishable. This can be seen more clearly in the derivative of the thermal conductance in Fig. IV.2(b).

The most relevant quantity determining the presence or the absence of the half plateaus appears to be $k_B\theta/E_L$ ratio. Since, for the saddle-potential model all steps have the same value for E_L, half-plateaus develop concurrently in all steps for certain range of values of this ratio. There are four different regimes with rough boundaries that can be distinguished in this model. A few representative plots belonging to some of these regimes are shown in Fig. IV.3.

(1) In the low temperature regime where $k_B\theta/\hbar\omega_x \lesssim 0.08$, there are no half plateaus. Moreover, the derivative $\partial K/\partial\mu$ has only a single peak at the steps. (2) In the intermediate temperature regime where $0.08 \lesssim k_B\theta/\hbar\omega_x \lesssim 0.4$, a double-peak structure develops in the derivative $\partial K/\partial\mu$. This is the parameter range where a structure with a smaller slope appears around the middle of the steps in the K versus μ graph. With increasing temperature, that slope goes down making the graph of K to have an almost flat shape at the high end of this regime. (3) In the high temperature regime where $0.4\hbar\omega_x \lesssim k_B\theta \lesssim \hbar\omega_y$, the derivative $\partial K/\partial\mu$ becomes much smaller around the middle of the steps (but does not vanish). As a result, K appears to be almost constant with increasing μ. This is the parameter range where the half-plateaus are present. Note that the shape of the graph of K is more like an extremum (a function whose first two derivatives is zero) rather than flat. A surprising feature is that the half plateaus become much more pronounced with increasing temperature as a result of the cooperation of two different effects. First, the slope of the plateau region goes further down, and second, the width of that region (e.g., peak to peak distance in the derivative graph) increases. Since the latter also implies that the widths of the integer plateaus decrease, half plateaus expand at the expense of integer plateaus as the temperature is increased. Towards the high end of this regime however, neighboring subbands start contributing to the conduction process causing the slope of the half plateaus to increase with increasing temperature (not shown). (4) Finally, at very high temperatures where $k_B\theta \gtrsim \hbar\omega_y$, the contribution of neighboring subbands is significant and

as a result both integer and half integer plateaus are wiped-out (not shown).

In order to understand the results summarized above, it is necessary to concentrate on the g_2 integral, which is the term in Eq. (IV.5) that provides the most significant contribution to K. The remaining term, g_1^2/g_0, is essential for including the effect of the Seebeck potential developed across the contact, but its contribution is almost always negligible except around the first step. For this reason, it is appropriate to investigate the derivative of g_2 which can be expressed as

$$\frac{\partial g_2}{\partial \mu} = \int x^2(-f'(x))T'(\mu + xk_B\theta)dx \quad .$$

Here $x^2(-f'(x))$ factor has a symmetric double-peak shape centered at $x = 0$, with peaks at $x \approx \pm 2.4$ and each peak having a width of order unity. On the other hand, $T'(\mu + xk_B\theta)$ factor has a single peak at each conductance step with widths of the order $E_L/k_B\theta$. The derivative of g_2 shows the same peak structure as one of these factors that has the greatest width. Therefore, when $E_L \ll k_B\theta$, $\partial g_2/\partial\mu$ has a double-peak structure at each step implying the presence of half plateaus, while in the opposite extreme, when $E_L \gg k_B\theta$, it has only a single peak. In the former case, the peak-to-peak distance is around $\Delta\mu = 2 \cdot 2.4 k_B\theta$ which means that the widths of the half-plateaus is proportional to the temperature.

The slopes of the half plateaus can also be calculated approximately as follows. To simplify the calculation, consider $\mu = E_n$ which corresponds to the midpoint of the $T = n$ to $T = n+1$ transition step. Although, the minimum of

$\partial K/\partial\mu$ is shifted to lower values of μ as can be seen in Fig. IV.3(b), derivative at the midpoints is sufficient for a rough representative value. Ignoring all other steps for simplicity, which amounts to the approximation $\hbar\omega_y \gg k_B\theta$, one can obtain

$$\frac{\partial g_2}{\partial \mu} = \frac{2\pi}{\hbar\omega_x}\int x^2(-f'(x))(-f'(\lambda x))dx = \frac{2\pi}{\hbar\omega_x}h(\lambda) \quad ,$$

where $\lambda = 2\pi k_B\theta/\hbar\omega_x$. A limiting value at the high temperatures, $k_B\theta \gg \hbar\omega_x$, can be obtained by employing the relation

$$h(\lambda) = \frac{1}{\lambda^3}h(\frac{1}{\lambda}) \quad ,$$

as $h(\lambda) \approx h(0)/\lambda^3$ resulting in the following

$$\frac{\partial g_2}{\partial \mu} \approx \frac{1}{48}\frac{(\hbar\omega_x)^2}{(k_B\theta)^3} \quad .$$

To be complete, the contribution of the terms arising from the Seebeck effect has to be included as well. With a similar analysis it can be found that

$$\frac{1}{K_0}\frac{\partial K}{\partial \mu} \approx \frac{1}{16\pi^2}\frac{(\hbar\omega_x)^2}{(k_B\theta)^3} + \frac{3\log^2 2}{4\pi^2}\frac{1}{(n+1/2)^2}\frac{1}{k_B\theta} \quad .$$

The restriction $\hbar\omega_y \gg k_B\theta \gg \hbar\omega_x$ and the fact that it gives the slope of only one point on a half plateau makes this expression of limited usefulness for practical cases. The only conclusion that should be drawn from this expression is that in the high-temperature regime where the half-plateaus are present, the slope tends to get smaller as the temperature is raised and it is inversely proportional to the temperature at best. Note that this is very large compared to the slopes of the integer plateaus, which has an exponential dependence on

inverse temperature. The main differences between the two types of plateaus comes to light with this result. Half plateaus may not be considered completely flat, but they tend to become flatter as the temperature is raised. In contrast, integer plateaus are considered completely flat when the transmission sum function, $T(E)$, is constant on the plateaus and this gets better as the temperature is lowered.

Finally, the value of the heat conductance at half-plateaus are found not to be exactly equal to the half-integer multiples of the conductance quantum as can be seen in Fig. IV.3(a). Starting from the second step, half-plateaus occur at conductance values $K \approx 1.40K_0$, $2.44K_0$, $3.46K_0$ and so on, approaching to half-integer multiples of K_0 as the number of conducting sub-bands increase. Numerical calculations indicate that these values are independent of all parameters of the problem. For this reason, in order to calculate the values of the conductance, $\omega_x \to 0$ limit can be considered to simplify the problem. In this limit, $T(E)$ has a step-function dependence on E. When the chemical potential is chosen at the midpoint of $T = n$ to $T = n + 1$ transition step, the values

$$g_0 = n + \frac{1}{2}, \quad g_1 = \ln 2, \quad g_2 = \frac{\pi^2}{3}(n + \frac{1}{2}),$$

can be found which give the conductance values

$$K = K_0 \left(n + \frac{1}{2} - \frac{3 \ln^2 2}{\pi^2} \frac{1}{n + \frac{1}{2}} \right) \qquad n = 1, 2, \ldots \quad .$$

Numerically calculated values are consistent with this expression.

Although the bimodal character of the kernel of the integral for g_2 is re-

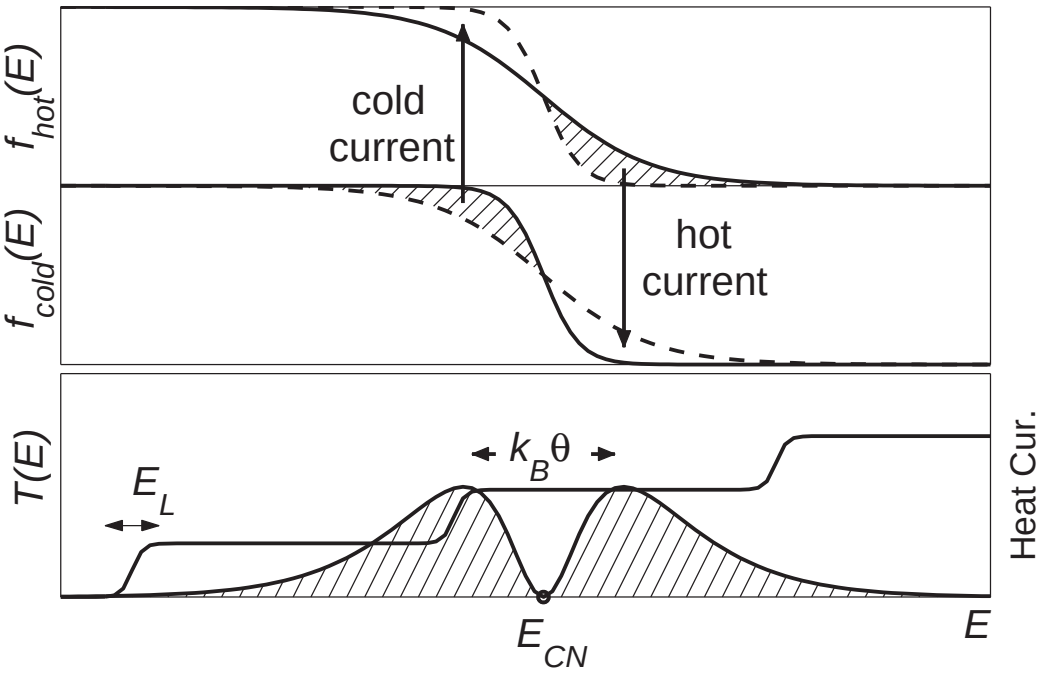

Figure IV.4: Currents between a hot (above) and a cold conductor (middle). The transmission sum function, $T(E)$, and the energy-resolved heat current (shaded curve) are plotted below. The current node, E_{CN}, the energy at which the current is zero, is present due to the restriction that the total particle current is zero. The relative shift of the Fermi levels due to the Seebeck effect is not shown.

sponsible for the half plateaus[15], there is a more straightforward explanation that involves uncomplicated physical terms. As illustrated in Fig. IV.4, when a hot and a cold conductor is connected so that there is no net electrical current between them, the distribution of electrons has the property that there are more electrons above the Fermi level in the hot conductor compared to the cold one. As a result, at these energies the particle current is from the hot to the cold conductor and they carry more energy than the Fermi energy (hot current). On the other hand, the cold conductor has more electrons with energy less than the Fermi level. For this reason these electrons flow from the cold to the hot conductor and therefore they carry energy smaller than the Fermi energy (cold current). Obviously both currents cause a net heat transfer from the hot to the cold conductors. The important point is that in between them there is some energy where there is no particle current. Note that there should inevitably be such a current node if the zero net electric current condition is satisfied, which is always the case for heat conductance measurements. Finally, when the gate voltage on the contact is changed, the transmission probabilities and the currents are altered. The two relevant energy scales are E_L, the energy range where the transmission probability is modified for small changes in the gate voltage, and $k_B\theta$, the distance between the hot and cold-current energies. In the case $E_L \ll k_B\theta$, when modification region crosses through the current node, the thermal current remains constant creating the half-plateau structure of the thermal conductance. It also follows from this argument that the width of the plateaus is proportional to the temperature. In the opposite

case, $E_L \gtrsim k_B\theta$ the current node cannot be resolved from the current peaks and no half plateaus appear.

In the argument above, the relative shift of the Fermi levels due to the Seebeck effect has to be taken into the account as it will move the current node away from the Fermi level. However, as long as the node does not deviate too much, the crossing of the node with steps is inevitable. This appears to be the case for the second and higher steps but not for the first one. In the case of the first step, only a negligible amount of current flows at electron energies E with $T(E) \approx 0$. The significant part of the current should flow at higher energies on the $T(E) \approx 1$ side of the step. The current node is necessarily pushed above the first step and for this reason crossing does not occur, which explains why there are no half plateaus at the first step. In order to quantify this idea, the current node energy is calculated. Starting from the current expression between energies E and $E + dE$ in the linear regime,

$$(f_{\text{hot}}(E) - f_{\text{cold}}(E))T(E)dE = \left(\frac{\partial f(E)}{\partial \mu}(-e)V + \frac{\partial f(E)}{\partial \theta}\Delta\theta\right)dE$$

and using the Seebeck coefficient, $V/\Delta\theta = k_B g_1/e g_0$, one can obtain the energy of the current node as

$$E_{\text{CN}} = \mu + k_B\theta\frac{g_1}{g_0} \quad .$$

Half plateaus occur when this energy and the subband minima cross, i.e., when $E_{\text{CN}} \sim E_n$. As can be seen, the current node deviates from the Fermi level only by an amount proportional to the Seebeck coefficient. It is known well that the Seebeck coefficient displays peaks at the steps and minima at

the plateaus, however it is large and non-zero at and below the first step[15]. For this reason, the deviation of the current node becomes very important in this last case, which can be seen in Fig. IV.5 where E_{CN} is plotted around the first step ($n = 0$). Although for low temperatures ($k_B\theta/\hbar\omega_x = 0.02$, 0.8 and 0.2) the current node does not deviate much from the Fermi level and it indeed crosses the step (E_{CN} becomes smaller than E_0), these cases belong to the low and intermediate temperature regimes where the half plateaus are not observed. For the high temperatures where there should have been half plateaus however ($k_B\theta/\hbar\omega_x = 0.4$, 0.6 and 0.8), the Seebeck effect pushes E_{CN} significantly above the Fermi level with the result that E_{CN} lies also above the subband minimum, E_0. Therefore, no crossing occurs at energies around the step and for this reason there is no half plateau. Although it is found that E_{CN} gets smaller with decreasing μ and it eventually crosses E_0, this happens for much lower values of μ so that practically there is no current flowing. In summary, for all parameter ranges there cannot be any half-plateau on the first step either because the temperature is too small so that the current node is not resolved, or because the current node cannot cross the step. Indeed, no unusual structure has been observed at this step either in K or in $\partial K/\partial\mu$ for all parameters that are investigated in this numerical study.

IV.4 Conclusions

The formation and evolution of half-plateau structures in the thermal conductance are described. They are the most significant aspect of the violation of

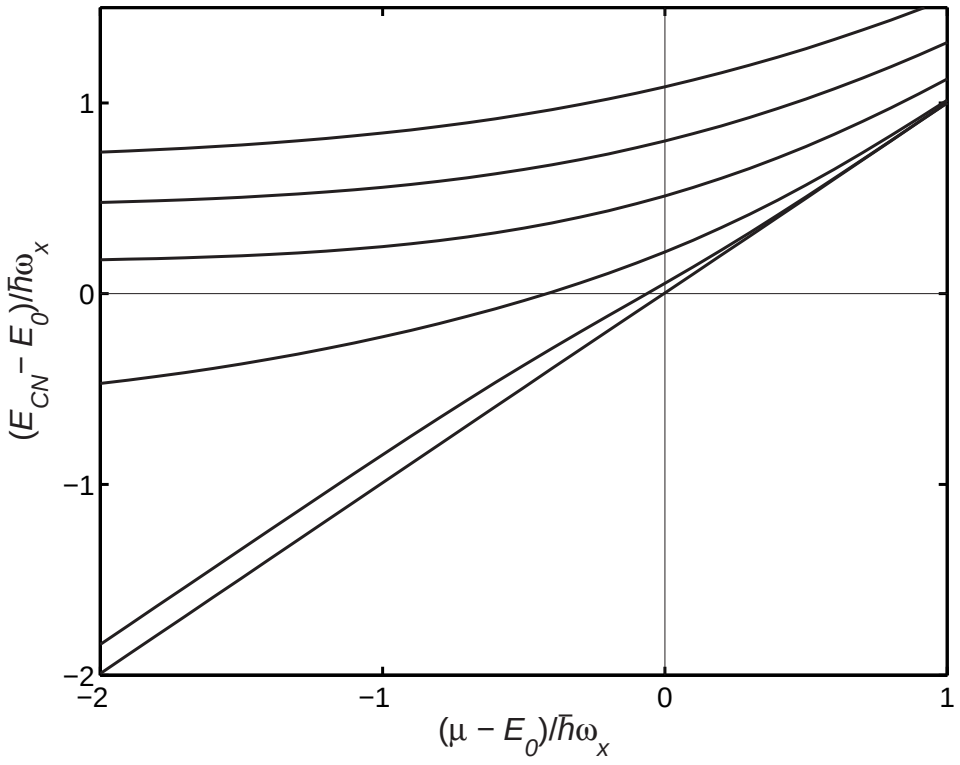

Figure IV.5: The energy of the current node as a function of the chemical potential for the first step. The effects of the other steps are ignored (i.e., $\omega_y \gg \omega_x$). The curves are obtained for (from bottom to top) $k_B\theta/\hbar\omega_x$ =0.02, 0.08, 0.2, 0.4, 0.6 and 0.8. For the lowest curve, E_{CN} is roughly equal to μ.

the Wiedemann-Franz law. The thermal distribution of energies of electrons contributing to a conduction process has a single-peak shape for electrical conductance measurements. In contrast, for thermal conductance measurements, it has a double-peak shape. If the transmission probability of a quantum point contact changes rapidly with electron energy, conductances become sensitive to the details of that distribution. Appearance of half plateaus in the thermal conductance is the most important result of that sensitivity.

The half plateaus appear in the temperature range $E_L \lesssim k_B\theta \lesssim E_T$. For this reason, a long contact with a smaller value of E_L increases the chances of experimental observation. Interestingly, half plateaus become more pronounced as the temperature is raised as they get wider and less steep at the low end of the temperature range above. Around $k_B\theta \sim E_T$, they start disappearing together with the integer plateaus, but due to their widths they are a little bit more distinguishable. The values of the conductance at the half plateaus are also evaluated and it is observed that these values are fixed, independent of the parameters of the contact. Although they are smaller than the exact half-integer multiples of the conductance quantum, they tend to approach to these values as the subband index increases. Finally, due to the strong effect of the Seebeck potential developed across the contact no half plateaus appear at the first step for any parameter values.

REFERENCES

[1] T. J. Thornton, M. Pepper, H. Ahmed, D. Andrews, G. J. Davies, Phys. Rev. Lett. **56** 1198 (1986).

[2] B. J. van Wees, L. P. Kouwenhoven, H. van Houten, C. W. J. Beenakker, J. E. Mooij, C. T. Foxon and J. J. Harris, Phys. Rev. B **38** 3625 (1988).

[3] D. A. Wharam, T. J. Thornton, R. Newbury, M. Pepper, H. Ahmed, J. E. F. Frost, D. G. Hasko, D. C. Peacock, D. A. Ritchie and G. A. Jones, J. Phys.: Solid State Phys. **21** L209 (1988).

[4] R. Landauer, Localization, Interaction and Transport Phenomena, Springer-Verlag, NY, 1985. R. Landauer, **1** 223 (1957). R. Landauer, Phil. Mag. **21** 863 (1970). R. Landauer, J. Phys.: Condens. Matter **1** 8099 (1989).

[5] M. Büttiker, Y. Imry, R. Landauer and S. Pinhas , **31** 6207 (1985).

[6] E. Tekman and S. Çıracı Phys. Rev. B **43** 7145 (1991).

[7] A. Szafer and A. D. Stone Phys. Rev. Lett. **62** 300 (1988).

[8] E. Castaño and G. Kirczenow, Phys. Rev. B **45** 1514 (1991).

[9] Hongqi Xu, Phys. Rev. B **48** 8878 (1993).

[10] D. van der Marel and E. G. Haanappel, Phys. Rev. B **39** 7811 (1989).

[11] J. Wróbel, F. Kuchar, K. Ismail, K. Y. Lee, H. Nickel and W. Schlapp, Surface Science **263** 261 (1992).

[12] L. G. L. Snider, M. S. Miller, M. J. Rooks and E. L. Hu, Appl. Phys. Lett. B **59** 2727 (1991).

[13] L. Olesen E. Lægsgaard, I. Stensgaard, F. Besenbacher, J. Schiøtz, P. Stoltze, K. W. Jacobsen and J. K. Nørskov, Phys. Rev. Lett. **72** 2251 (1994).

[14] R. Taboryski, A. Kristensen, C. B. Sørensen and P. E. Lindelof, Phys. Rev. B **51** 2282 (1994).

[15] H. van Houten and C. Beenakker, Physics Today, 22 (July 1996).

[16] Imry Y, *'Introduction to Mesoscopic Physics'* (Oxford University Press, New York, 1997)

[17] S. Datta, '*Electronic Transport in Mesoscopic Systems'* eds. H. Ahmed, M. Pepper, A. Broers, (Cambridge University Press, UK. 1995)

[18] Onsager L., Phys Rev. **37** 405 (1937)

[19] L. G. C. Rego, G. Kirczenow, *Phys. Rev. Lett.*, **81**, (1998), 232-235.

[20] L. G. C. Rego, G. Kirczenow, *Phys. Rev. B*, **59**, (1998), 13080-6.

[21] K. Schwab *et al.*, *Nature*, **404**, (2000), 974-6.

[22] K. Schwab *et al.*, *Physica E*, **9**, (2001), 60-68.

[23] P. Streda, J. Phys.: Condensed Matter **1**, 1025 (1988).

[24] C. R. Proetto, Phys. Rev. B **44**, 9096 (1991).

[25] H. van Houten, L. W. Molenkamp, C. W. J. Beenakker, C. T. Foxon, Semicond. Sci. Technol. **7**, B215 (1992).

[26] L. W. Molenkamp, H. van Houten, C. W. J. Beenakker, R. Eppenga, C. T. Foxon, Phys. Rev. Lett. **65**, 1052 (1990).

[27] L. W. Molenkamp, Th. Gravier, H. van Houten, O. J. A. Buijk, M. A. A. Mabesoone, C. T. Foxon, Phys. Rev. Lett. **68**, 3765, (1992).

[28] Z.-S. Ma, L. Schülke, Phys. Rev. B **59**, 13209 (1998).

[29] Z.-S. Ma, J. Wang, H. Guo, Phys. Rev. B **59**, 7575 (1999).

[30] Z.-S. Ma, H. Guo, L. Schülke, Z.-Q. Yuan, H.-Z. Li, Phys. Rev. B **61**, 317 (2000).

[31] B. Qiao, H. E. Ruda, Z. Xianghua, Physica A **311**, 429 (2002).

[32] T. N. Todorov, J. Phys.: Condensed Matter **12**, 8995 (2000).

[33] E. N. Bogachek, A. G. Scherbakov and U. Landman, Solid State Comm. **108**, 851 (1998).

[34] E. N. Bogachek, A. G. Scherbakov and U. Landman, Phys. Rev. B **60**, 11678 (1999).

[35] A.E. Krishnaswamy, S.M Goodnick, M.N. Wyborne, C. Berven, Microelectronic Engineering **63**, 123 (2002).

[36] A. S. Dzurak, C. G. Smith, L. Martin-Moreno, M. Pepper, D. A. Ritchie, G. A. C. Jones, and D. G. Hasko, J. Phys: Condens. Matter **5**, 8055 (1993).

[37] M. Büttiker, J. Phys: Condens Matter **5**, 9361 (1993).

[38] U. Sivan and Y. Imry, Phys. Rev. B **33**, 551 (1986).

[39] B. J. van Wees, H. van Houten, C. W. J. Beenakker, J. G. Williamson, L. P. Kouwenhoven, D. van der Marel, and C. T. Foxon, Phys. Rev. Lett. **60**, 848 (1988).

[40] D. A. Wharam, T. J. Thornton, R. Newbury, M. Pepper, H. Ahmed, J. E. F. Frost, D. G. Hasko, D. C. Peacock, D. A. Ritchie, and G. A. C. Jones, J. Phys. C: Solid State Phys. **21**, L209 (1988).

[41] R. Landauer, Philos Mag. **21**, 863 (1970).

[42] L. W. Molenkamp, Th. Gravier, H. van Houten, O. J. A. Buijk, M. A. A. Mabesoone and C. T. Foxon, Phys. Rev. Lett. **68**, 3765 (1992).

[43] L. I. Glazman and A. V. Khaetskii, Europhys. Lett. **9**, 263 (1989).

[44] Hongqi Xu, Phys. Rev. B, **47**, 15630 (1993).

[45] N. K. Patel, J. T. Nicholls, L. MartínMoreno, M. Pepper, J. E. F. Frost, D. A. Ritchie and G. A. C. Jones, Phys. Rev. B **44**, 13549 (1991).

[46] J. E. F. Frost, K.F. Berggren, M. Pepper, M. Grimshaw, D. A. Ritchie, A. C. Churchill and G. A. C. Jones, Phys. Rev. B **49**, 11500 (1994).

[47] U. Sivan and Y. Imry, Phys. Rev. B **33**, 551 (1986).

[48] M. Büttiker, Phys. Rev. B **41**, 7906 (1989).

[49] J. N. L Connor, Mol. Phys. **15**, 37 (1968).

[50] H. A. Fertig and B. I. Halperin, Phys. Rev. B **36**, 7969 (1987).

VITA

M. Ali ÇİPİLOĞLU was born in Manisa in 1971. After having graduated from İzmir Atatürk High School in 1989, at the same year he joined to Physics department of Dokuzeylül University as a B.Sc. student and received his bachelor's degree in 1994. Just after completing master's program at Celal Bayar University in the Department of Physics in 1997, he has been accepted as a Ph.D. student at Middle East Technical University. He worked as a research assistant at Celal Bayar University during the period between 1995 and 1997. He has been, then, employed at Middle East Technical University as a research assistant since January 1999.